Chemical Science

ROYAL SOCIETY OF CHEMISTRY

REVIEW

View Article Online
View Journal | View Issue

Cite this: *Chem. Sci.*, 2024, **15**, 7848

Structure regulation and synchrotron radiation investigation of cathode materials for aqueous Zn-ion batteries

Shiqiang Wei,[a] Yixiu Wang,[a] Shuangming Chen *[a] and Li Song [ab]

In view of the advantages of low cost, environmental sustainability, and high safety, aqueous Zn-ion batteries (AZIBs) are widely expected to hold significant promise and increasingly infiltrate various applications in the near future. The development of AZIBs closely relates to the properties of cathode materials, which depend on their structures and corresponding dynamic evolution processes. Synchrotron radiation light sources, with their rich advanced experimental methods, serve as a comprehensive characterization platform capable of elucidating the intricate microstructure of cathode materials for AZIBs. In this review, we initially examine available cathode materials and discuss effective strategies for structural regulation to boost the storage capability of Zn^{2+}. We then explore the synchrotron radiation techniques for investigating the microstructure of the designed materials, particularly through *in situ* synchrotron radiation techniques that can track the dynamic evolution process of the structures. Finally, the summary and future prospects for the further development of cathode materials of AZIBs and advanced synchrotron radiation techniques are discussed.

Received 14th January 2024
Accepted 1st May 2024

DOI: 10.1039/d4sc00292j

rsc.li/chemical-science

1 Introduction

With the escalating energy demand, alternative energy sources, such as solar, tidal and wind energy, are poised to assume an increasingly critical role within the energy landscape.[1,2] In this scenario, increased demands and standards are being imposed on energy storage devices deployed in energy hub stations.[3] The plentifulness, security, and sustainability of resources for energy storage devices necessitate scrupulous examination.[4] While organic lithium-ion batteries (LIBs) have achieved considerable success, it remains necessary to explore and develop supplemental energy storage devices to meet large-scale requirements.[5] Aqueous Zn-ion batteries (AZIBs) are widely expected to hold significant promise, due to the advantages of low cost, environmental sustainability, and high safety.[6–8] The development of AZIBs closely relates to the properties of cathode materials. However, the availability of suitable cathode materials poses a challenge in expanding AZIBs due to the strong interaction between Zn^{2+} and the lattice as well as an aqueous environment.

So far, numerous cathode materials have been developed including those based on vanadium, manganese, Prussian blue analogues, and other materials.[9–11] Vanadium-based oxides are considered promising cathode materials due to their high-capacity characteristics. However, their practical application is hindered by their inadequate stability and voltage plateau.[12] While manganese-based oxides exhibit improved voltage plateau, their dissolution in the aqueous solution is significantly exacerbated by the Jahn–Teller distortion phenomenon.[13] Prussian blue analogs exhibit an advantageous open 3D structure and adjustable elemental composition, making them excellent candidates for Zn^{2+} storage materials. Nevertheless, the limited capacity of these materials hampers their competitiveness.[14] Additionally, various other cathode materials are under development for AZIBs, such as sulfur,[15] MXenes,[10,16,17] and organic compounds.[18] To boost the Zn^{2+} storage capability of the aforementioned materials, numerous effective strategies for structural regulation have been employed. Among these, interlayer engineering offers a promising strategy for increasing the interlayer spacing while maintaining the structural stability of layered materials. Defect structures not only create extra active sites but also allow for the modulation of the electronic structure of electrode materials. Doping strategies optimise the intrinsic electronic structure of electrode materials, resulting in improved conductivity and enhanced structural stability. In addition, compositional design enhances both the stability of cathode materials and the formation of a heterogeneous interfacial layer that facilitates electron transfer.[19] Furthermore, electrolyte regulation, as another effective approach, can simultaneously enhance the stability and migration behaviour of Zn^{2+} in both the cathode and anode.[20] The designed microstructures and their action mechanism play a crucial role in determining the electrochemical performance. Typically, the

[a]*National Synchrotron Radiation Laboratory, CAS Center for Excellence in Nanoscience, University of Science and Technology of China, Hefei 230029, P. R. China. E-mail: csmp@ustc.edu.cn*

[b]*Zhejiang Institute of Photonelectronics, Jinhua 321004, Zhejiang, P. R. China*

design of these microstructures is achieved by empirical or trial-and-error approaches. Therefore, establishing a direct correlation between the modified material's microstructure and its electrochemical performance using advanced characterization techniques is essential for accurate design.

Synchrotron radiation light source offers a wide spectrum of light with high brightness and excellent collimation, providing an effective material characterization platform.[21] Among various techniques, synchrotron radiation X-ray diffraction technology utilizes concentrated light, enabling high spatial resolution testing that surpasses the capabilities of conventional X-ray diffraction. It serves as an effective approach for finely characterizing the microstructure of electrode materials. Additionally, the high flux of synchrotron radiation X-rays allows for millisecond-level temporal resolution, facilitating high-time-resolved *in situ* monitoring of the phase transition behaviour during battery reaction processes.[22] Synchrotron radiation X-ray absorption spectroscopy (XAS) is a crucial technique for investigating the local structural properties, valence states, and their dynamic evolution processes under operating conditions of electrode materials.[23] Besides, other synchrotron radiation techniques are continuously emerging; for instance, synchrotron X-ray fluorescence microscopy (XFM) is a reliable and non-destructive technique that allows for elemental mapping and identification of potential chemical elements.[24] In conclusion, synchrotron radiation techniques have gradually become advanced characterization methods for investigating the microstructures of electrochemical energy materials, electrode interfaces, and their evolution patterns.

To advance the exploration of high-performance cathode materials, it is imperative to acquire a comprehensive understanding of the relationships between their microstructure and performance. In this review, we will begin with delivering an all-inclusive review of the common cathode materials for AZIBs and the most effective strategies for structural regulation to obtain a competitive performance. Subsequently, synchrotron radiation techniques will be employed to investigate the engineered structure and track its dynamic evolution process using *in situ* methodologies. This review contributes to a deeper understanding of the structure–performance relationship for cathode materials in AZIBs by emphasizing the structure regulation and synchrotron radiation investigation, thereby facilitating the materials'-controlled fabrication and rational regulation (Fig. 1).

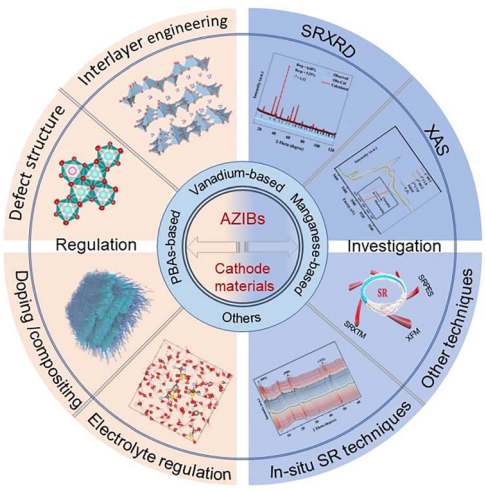

Fig. 1 Schematic illustration of structure regulation and synchrotron radiation investigation of cathode materials for AZIBs.

2 Cathode materials

In AZIBs, the cathode materials play a crucial role in determining the energy and power densities of the associated devices. In recent years, significant progress has been made in developing cathode materials, with the goal of enhancing the Zn^{2+} storage capability. Nevertheless, disparities remain between the current state and practical implementation, thereby prompting a growing inclination toward allocating greater endeavors to the advancement of high-performance cathode materials. This section examines the common cathode materials used for AZIBs, including vanadium-based, manganese-based, Prussian blue analogue-based, and other cathode materials.

2.1 Vanadium-based cathodes

Vanadium-based cathode materials have garnered considerable attention for AZIBs in recent years. Vanadium-based materials possess several advantages, including abundance, low cost, and excellent compatibility with AZIB systems. Due to the multiple valence states of vanadium (V^{2+}, V^{3+}, V^{4+}, V^{5+}) and distinct crystal structures, a diverse range of vanadium-based compounds have been developed, involving multiple electron transfer reactions during electrochemistry. These compounds demonstrate enhanced battery capacity, making them a promising choice as cathode materials for AZIBs.[25] Specifically, for the cathode of AZIBs, vanadium-based oxides, vanadium phosphates, and oxygen-free vanadium-based materials have been the preferred choices.[26]

Vanadium-based oxides are highly desirable compared to other vanadium-based compounds. The representative cathode material, V_2O_5, possesses a layered structure composed of distorted [VO_5] square pyramids that stack in an alternating

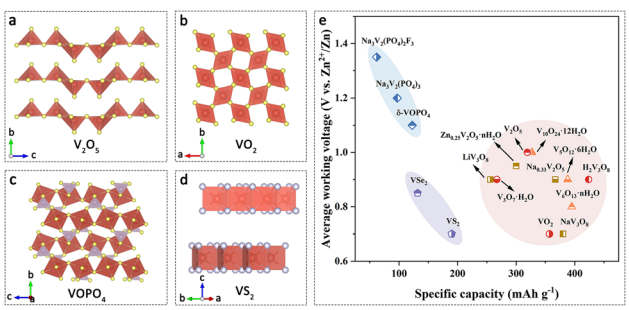

Fig. 2 Vanadium-based cathodes. The crystal structures of (a) V_2O_5, (b) VO_2, (c) $VOPO_4$ and (d) VS_2. (e) Average working voltages *versus* specific capacities of representative vanadium-based cathode materials for AZIBs. Data from ref. 29, 32, 35 and 37–49.

manner (up–down–up–down) through shared edges and corners. Each layer is aligned along the *c*-axis (Fig. 2a), resulting in an inherent interlayer spacing for intercalating Zn^{2+}. When employed as a cathode material for AZIBs, the V_2O_5 electrode exhibits an initial specific capacity of 323 mA h g^{-1} at a working voltage range of 0.2–1.6 V in a 3 M $Zn(CF_3SO_3)_2$ electrolyte. After 15 cycles, the capacity increases to 470 mA h g^{-1}.[27] However, this layered structure is prone to structural collapse during repeated insertion/extraction of Zn^{2+} ions, and it fails to provide sufficient active sites for effective charge storage, resulting in capacity degradation.[28]

Tunnel-like structured vanadium oxides also demonstrate the ability to facilitate rapid insertion/extraction of Zn^{2+} ions. VO_2 is composed of distorted [VO_6] octahedra that form a framework of tunnel-like channels through shared edges/corners (Fig. 2b). This structure undergoes minimal changes during Zn^{2+} ion intercalation, contributing to improved structural stability in AZIBs. Furthermore, the one-dimensional tunnels present in VO_2 provide convenient pathways for the insertion of Zn^{2+}, enabling fast charge–discharge processes.[29] However, the energy storage mechanism of VO_2 in AZIBs remains controversial.[30] Additionally, the strong electrostatic interaction between Zn^{2+} ions and the host material results in the formation of "dead Zn" regions within the crystal structure, leading to a decrease in battery capacity and cycling performance.[31] As an alternative tunnel-like structured cathode material, V_6O_{13} consists of layers of vanadium oxide with mixed valence states of V^{4+} and V^{5+}, providing a higher number of active sites. It can be considered as a combination of monolayer V_2O_5 and bilayer VO_2.[32] Shan *et al.* reported that the V_6O_{13} cathode demonstrates good cycling stability, maintaining a capacity of 206 mA h g^{-1} after 3000 cycles at a current density of 10 A g^{-1} within a working voltage range of 0.3–1.4 V.[33] Furthermore, V_2O_3 with a three-dimensional tunnel-like structure, attributed to its corundum-type structure, exhibits metallic behavior and low electrical resistance. It demonstrates favorable rate performance (207 mA h g^{-1} at 0.1 A g^{-1}) and cycling stability (82.1% capacity retention after 2500 cycles under 3 A g^{-1}) within a working voltage range of 0.2–1.6 V.[34]

Phosphate-based materials, known for their high-performance as cathode materials in lithium-ion batteries and sodium-ion batteries, have recently been applied as cathode materials in AZIBs. Among them, vanadium phosphate ($VOPO_4$) cathode materials exhibit various crystal structures and higher discharge plateaus, effectively enhancing the energy density of AZIBs (Fig. 2c). Zhao *et al.* prepared a δ-$VOPO_4$ cathode material with a high discharge plateau (1.46 V *vs.* Zn^{2+}/Zn), but lower specific capacity (122.6 mA h g^{-1} at 1C).[35] In recent years, materials with a Na superionic conductor (NASICON) structure have gained significant attention as cathode materials due to their excellent structural stability and large interstitial channels with high ionic migration rates.[36] $Na_3V_2(PO_4)_3$, as a typical example, achieved a higher working voltage plateau (1.40 V *vs.* Zn^{2+}/Zn), but exhibited a lower capacity (97 mA h g^{-1} at 0.5C) in AZIBs.[37] Despite the higher voltage plateau offered by vanadium phosphate cathodes, their application in AZIBs is still limited by several drawbacks, including low electronic conductivity, low capacity, and poor capacity retention at low current densities.

Oxygen-free vanadium-based cathode materials, such as vanadium sulfide (VS_2), vanadium carbide (V_2C), and vanadium selenide (VSe_2), possess high electronic conductivity and layered structures with large interlayer spacing. These characteristics effectively mitigate the electrostatic interaction with Zn^{2+}, enabling reversible Zn^{2+} insertion/extraction. He *et al.* first investigated the energy storage properties of layered VS_2 (Fig. 2d) in AZIBs, which shows a capacity of 190.3 mA h g^{-1} at the current density of 0.05 A g^{-1} within a voltage range of 0.4–1.0 V.[38] Wu *et al.* studied the Zn^{2+} storage and mechanisms in few-layer ultrathin VSe_2, achieving a discharge plateau at 1.0–0.7 V and a specific capacity of 131.8 mA h g^{-1} at the current density of 0.1 A g^{-1}.[39] Our group prepared freestanding films of porous delaminated V_2C–MXenes and carbon nanotube composites, demonstrating excellent performance in aqueous zinc-ion hybrid supercapacitors within a voltage range of 0.1–1.1 V (190.2 F g^{-1} at 0.5 A g^{-1}).[10]

Despite the low cost, multi-electron transfer capability, and high capacity of vanadium-based materials, they still face certain challenges that hinder their practical application in AZIBs, including low working voltages (Fig. 2e), structural degradation during cycling, and diminished electrochemical performance caused by surface element dissolution or phase transitions. Therefore, it is crucial to further enhance these materials through modifications that can provide an ample number of active sites within the crystal structure and facilitate rapid storage pathways for Zn^{2+} ions. Additionally, a comprehensive understanding of the energy storage mechanisms is imperative to overcome these limitations and fulfill the demands of practical applications.

2.2 Manganese-based cathodes

Manganese-based materials have been extensively studied as cathode materials for AZIBs due to their abundant resources, low cost, moderate working voltage, and high theoretical capacity. Among them, manganese-based oxides (MnO, MnO_2, Mn_2O_3, and Mn_3O_4) have gained significant attention as cathode materials for AZIBs, owing to their diverse crystal structures and the multiple oxidation states of manganese.[50]

Manganese dioxide (MnO_2) is composed of [MnO_6] octahedra that form different crystal structures through shared corners or edges. These structures include tunnel structures (α-MnO_2, β-MnO_2, γ-MnO_2, *etc.*), layered structures (δ-MnO_2), and three-dimensional (3D) structures (λ-MnO_2 and ε-MnO_2) (Fig. 3a–d). The operating voltage window of MnO_2 cathode materials in AZIBs typically ranges from 1.0 to 1.8 V, providing a voltage plateau of around 1.2 V. In the tunnel-type MnO_2, α-MnO_2 exhibits a (2 × 2) tunnel structure and demonstrates an initial discharge capacity of 233 mA h g^{-1} at a current density of 83 mA g^{-1}.[51] However, β-MnO_2, characterized by a (1 × 1) tunnel structure, possesses narrower tunnels that hinder the diffusion of Zn^{2+} ions.[52] It has been demonstrated that β-MnO_2 undergoes a transformation into layered zinc buserite following the initial discharge cycle.[53] γ-MnO_2 possesses a mixed (1 × 1)

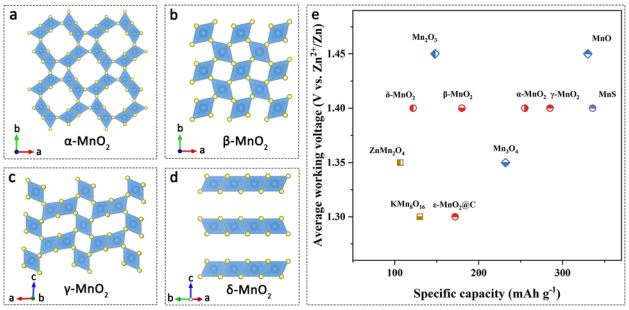

Fig. 3 Manganese-based cathodes. The crystal structures of (a) α-MnO_2, (b) β-MnO_2, (c) γ-MnO_2, (d) δ-MnO_2. (e) Average working voltages *versus* specific capacities of representative manganese-based cathode materials for AZIBs. Data from ref. 54, 55, 57, 58, 60, 61 and 63–67.

and (1 × 2) tunnel structure, which provides better Zn^{2+} diffusion capacity compared to β-MnO_2. It exhibits an initial discharge capacity of 285 mA h g^{-1} at 0.05 mA cm^{-2}.[54] For the layered-type, δ-MnO_2 owns a large interlayer spacing which enables enhanced Zn^{2+} ion storage capacity (122 mA h g^{-1} at 83 mA g^{-1}).[55] For the 3D-type MnO_2, λ-MnO_2 and ε-MnO_2 exhibit dense packing structures, resulting in lower capacity during Zn^{2+} ion insertion/extraction mechanisms. For enhancing the ability of Zn^{2+} storage, Sun *et al.* synthesized a nanocrystalline ε-MnO_2 cathode, which shows a high capacity of 290 mA h g^{-1} at 0.3C.[56] These studies emphasize the diverse crystal structures of MnO_2 and their influence on the electrochemical performance in AZIBs.

Other types of manganese-based oxides, like MnO, which has the lowest oxidation state, can also be used as a cathode material for AZIBs. During the initial charging process, MnO undergoes an irreversible phase transition to layered δ-MnO_2, which is a kind of electrochemical activation and achieves a high capacity of 330 mA h g^{-1} at a current density of 0.1 A g^{-1}. It exhibits cycling stability with 80.7% capacity retention after 300 cycles at a current density of 0.3 A g^{-1}.[57] Unlike the irreversible phase transition, Mn_2O_3 undergoes a reversible phase transition between layered zinc birnessite and α-Mn_2O_3 structures during the charge–discharge process, resulting in a capacity of 148 mA h g^{-1} at a current density of 0.1 A g^{-1}.[58] Mn_3O_4, generally considered as a mixture of MnO and Mn_2O_3, exists in a spinel phase.[59] It undergoes phase transitions to intermediate Mn_5O_8 and finally to Zn-birnessite during the charge–discharge process, achieving a capacity of 232 mA h g^{-1} at a current density of 0.2 A g^{-1} within the voltage range of 0.8–1.9 V.[60] Oxygen-free MnS has been introduced as another type of manganese-based cathode material in recent years for AZIBs. However, Chen *et al.* has found that the electrochemical activation on the intrinsically inactive α-MnS transforms it into manganese oxide suitable for AZIBs. The manganese oxide derived from MnS exhibits better Zn ion diffusion kinetics and a higher electrochemically active surface area. It demonstrates a high specific capacity of 335.7 mA h g^{-1} with nearly 100% capacity retention after 100 cycles at 1C.[61]

While manganese-based cathode materials exhibit a high working voltage plateau (Fig. 3e), challenges such as manganese dissolution, phase transition, and structural transformation during cycling remain significant hurdles in the development of AZIBs.[62] These drawbacks can lead to structural collapse of the manganese-based materials, resulting in rapid capacity decay, poor rate capability and stability. Therefore, the development of structural optimization strategies is crucial in addressing these issues.

2.3 Cathodes based on Prussian blue analogues

Prussian blue analogues (PBAs), as typical metal–organic framework materials, are considered promising cathode materials for AZIBs due to their three-dimensional open frameworks, multiple active sites, non-toxicity, and low cost.[68] The structure of PBAs primarily consists of $MFe(CN)_6$ (M = Zn, Cu, Co, Ni, *etc.*), which exhibits a face-centered cubic structure with the *Fm3m* space group (Fig. 4a and b). It manifests as an open cage-like structure that facilitates the insertion/extraction of Zn^{2+} ions.[69] These materials with stable framework structures can achieve higher operating voltages and energy densities.

Zinc hexacyanoferrate (ZnHCF) PBAs have been applied into AZIBs as cathode materials by Zhang *et al.*, achieving an average operating voltage of 1.7 V and an energy density of 100 W h kg^{-1} at a power density of 0.1 kW kg^{-1}.[70] Trócoli *et al.* reported a copper hexacyanoferrate (CuHCF) used in AZIBs, reaching an average specific power density of 52.5 W kg^{-1}, with an average discharge potential of 1.73 V.[71] Among cathode materials for AZIBs, PBAs exhibit the highest operating voltage, but low capacity (Fig. 4d). Generally, the cathode electrode of PBAs delivers a specific capacity of no more than 100 mA h g^{-1} in the routine AZIB system.[69] For example, the $Zn_3[Fe(CN)_6]_2$ cathode material shows a specific capacity of 66.5 mA h g^{-1} at 0.06 A g^{-1} in a 3 M $ZnSO_4$ electrolyte based aqueous device.[72] Therefore, the design of composite materials and surface modifications have become promising directions for material modification.[73]

2.4 Other cathodes

In addition to the aforementioned cathode materials, various other types of cathode materials have also been employed in AZIBs, such as organic compounds, metal–organic frameworks

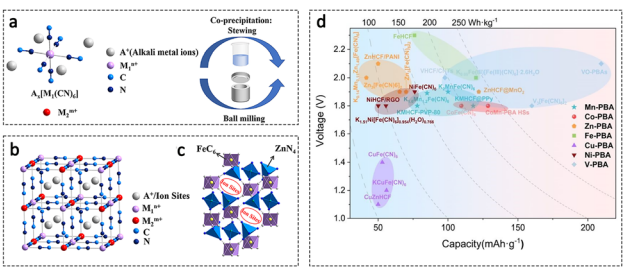

Fig. 4 Cathodes based on Prussian blue analogues. (a) The schematic diagram of PBA preparation; (b) the ideal structures of cubic PBAs; (c) the ideal rhombohedral structures of ZnHCF. Adapted from ref. 74, copyright 2022, Elsevier Ltd. (d) Comparison of PBAs applied to AZIBs. Adapted from ref. 75, copyright 2024, The Royal Society of Chemistry.

(MOFs), transition metal layered sulfides, and others. Organic compounds offer advantages such as low cost, high synthetic availability, and structural diversity compared to inorganic materials. Bipolar types of conductive polymers (CPs) were the earliest organic electrode materials used in AZIBs, including polyaniline (PANI), polypyrrole (PPy), polythiophene (PTh), poly(3,4-ethylenedioxythiophene) (PEDOT), and others. Among them, PANI is the most typical cathode material to date. Wan *et al.* utilized PANI/carbon felts as the cathode materials in AZIBs, achieving a capacity of 95 mA h g^{-1} at the current density of 5 A g^{-1} and an operating voltage of approximately 1.1 V *vs.* Zn^{2+}/Zn.[76] However, the unstable structure and poor electronic conductivity of organic electrode materials result in low capacity and inferior rate performance. Ye *et al.* proposed a novel poly(phenazine-*alt*-pyromellitic anhydride) (PPPA), which demonstrated an exceptionally high Zn^{2+} diffusion coefficient attributed to the extended π-conjugated plane within the PPPA structure.[77] MOFs possess highly porous structures, tunable frameworks, and multifunctionality, making them potential cathode materials for AZIBs.[78] Pu *et al.* synthesized several MOF materials and applied them as cathodes in AZIBs. High-performance AZIBs were constructed using Mn(BTC) MOF cathodes and ZIF-8-coated Zn (ZIF-8@Zn) anodes, achieving a capacity of 112 mA h g^{-1} at current densities of 50 mA g^{-1} in a voltage window of 1.0–1.9 V.[79] Transition metal sulfides and selenides with two-dimensional layered structures have been widely applied as anode materials in lithium-ion and sodium-ion batteries.[80] Although these materials have been investigated as cathode materials in AZIBs, such as MoS_2 and VSe_2, low capacity and operating voltage are still challenges for their further development.[81] Therefore, it is vital to introduce structure regulations to improve their electrochemical properties.

In order to enhance the energy density of AZIBs, sulfur (S), which has a high specific capacity (1675 mA h g^{-1}), is considered to be a promising cathode material. S cathodes exhibit a conversion-type reaction mechanism and effectively mitigate electrostatic interactions with Zn^{2+}, resulting in higher specific capacity and energy density.[15] Luo *et al.* infiltrated S into Ketjen Black (KB) to prepare the KB–S composite material, achieving a high-capacity of 1668 mA h g^{-1} and a high energy density of 1083.3 W h kg^{-1} with a discharge voltage platform of 0.7 V.[82] Significant breakthroughs have been made in the research of S cathodes, but it is crucial to solve the problems of slow reaction kinetics, volume expansion, cycling stability and by-products while ensuring high capacity and high energy density. With the same conversion-type reaction mechanism as the cathode material, iodine has been developed due to its advantages of low cost, non-toxicity, high energy density and multi-electron conversion reaction. The iodine cathode is capable of providing a high voltage platform of 1.3 V with high theoretical capacity (211 mA h g^{-1}) and energy density (322 W h L^{-1}).[83] Pan *et al.* used activated carbon fibre cloth adsorbed with iodine as the positive electrode to achieve a high capacity of 174.4 mA h g^{-1} (1C) at an average voltage of 1.22 V. In turn, the researchers further explored hosts with higher conductivity, spatial confinement structure and adsorption sites.[84] Li *et al.* employed Nb_2CT_x–MXene as a conductive host doped with I_2, realizing an ultra-flat voltage platform of 1.3 V and excellent multiplicative performance (143 mA h g^{-1} at 18 A g^{-1}).[85] However, due to the inherent poor electrical conductivity of iodine and the phase transition mechanism based on two-electron transfer, the slow kinetics, the shuttling effect of the polyiodide species and the by-products on the zinc anode still remain to be solved.

3 Structure regulation

Structure regulation has been employed to enhance the Zn^{2+} storage capability of cathode materials. The primary objective is to increase the number of active sites and improve the reversibility of the material framework. This section explores the most effective regulatory strategies that have been recently reported, with a particular emphasis on their methods, effects, and underlying mechanisms.

3.1 Interlayer engineering regulation

Layered materials have garnered significant interest for their potential application as cathodes in AZIBs due to their 2D structure, which facilitates rapid ion diffusion and enables smooth phase transitions during Zn^{2+} ion de/intercalation processes. Interlayer engineering represents a viable approach to expand the interlayer spacing while stabilizing the structural integrity of layered materials. Various intercalation agents, including H_2O molecule, metal ions, non-metallic ions, and organic polymers, have been extensively utilized to finely control the structural properties of layered cathode materials. Water molecules readily intercalate into layered materials during the preparation process, providing a "lubricating" effect. Yan *et al.* have demonstrated the significant influence of structural H_2O in a $V_2O_5 \cdot nH_2O$ cathode on Zn^{2+} ion chemistry (Fig. 5a). The findings indicate that H_2O molecules greatly reduce the effective charge and subsequently mitigate

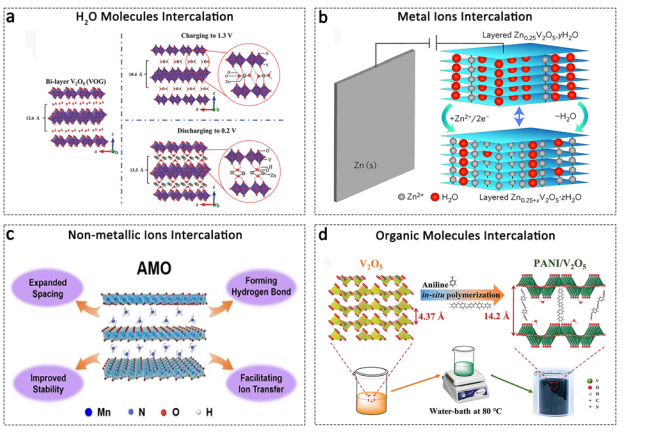

Fig. 5 Interlayer engineering regulation. (a) H_2O molecule intercalation into the V_2O_5 cathode. Adapted from ref. 86, copyright 2017, Wiley-VCH. (b) Zn^{2+} metal ion intercalation into the V_2O_5 cathode. Adapted from ref. 40, copyright 2016, Springer Nature. (c) Non-metallic NH_4^+ ion intercalation into MnO_2. Adapted from ref. 100, copyright 2023, Wiley-VCH. (d) Schematic illustration of the organic molecule's intercalation into the V_2O_5 cathode. Adapted from ref. 103, copyright 2021, Wiley-VCH.

electrostatic interactions with the V_2O_5 framework, thus facilitating its diffusion. The AZIB device based on $V_2O_5 \cdot nH_2O$ achieves an impressive energy density of 144 W h kg^{-1} (calculated based on the cathode and a 200% Zn anode).[86]

The insertion of cations with a large ionic radius as guest pillars would expand the interlayer spacing, while simultaneously enhancing the structural stability through electrostatic attraction between the cation and the adjacent layers. It appears that the presence of metal ions could induce the stretching of the interlayer spacing, while simultaneously exerting a pulling force on the adjacent layers to prevent structural collapse. The first-class cations comprise alkali ions, including Li^+, Na^+, and K^+, which function as pillars to stabilize the layered structures. Previous studies have demonstrated that the electrochemical performance of pre-intercalated cathodes is closely associated with the radius of the alkali ions. Zhang *et al.* employed a rapid molten-salt method to prepare a series of alkali metal ions pre-intercalated $M_xV_3O_8$ (M represents Li, Na, K). Due to the larger radius of K^+ compared to Li^+ and Na^+, the KVO structure exhibits the largest interlayer gallery, facilitating the diffusion of Zn^{2+} within this gallery. Consequently, the KVO cathode achieves a high capacity of 386 mA h g^{-1} at 0.1 A g^{-1}, surpassing that of the Li^+ and Na^+-based counterparts.[87] The second-class cations refer to various multivalent metal ions that have been pre-intercalated into the interlayer of layered materials, acting as interlayer pillars with stronger traction agents. These include Zn^{2+}, Mn^{2+}, Co^{2+}, Ni^{2+}, Mg^{2+}, Ca^{2+}, and others, which have been introduced into the interlayers.[40,88–92] As depicted in Fig. 5b, Kundu *et al.* presented a vanadium oxide bronze, pillared with interlayer Zn^{2+} ions and water ($Zn_{0.25}V_2O_5 \cdot nH_2O$), as the cathode material for a zinc-based cell. The study revealed a reversible Zn^{2+} ion de/intercalation process, exhibiting rapid kinetics and achieving a capacity of up to 300 mA h g^{-1}, which corresponds to more than one Zn^{2+} ion per formula unit.[40] However, the propensity of these intercalated cations to leach from the host materials is inevitable due to their weak interaction with negatively charged Helmholtz planes within the hosts and the inherent shearing/bulking effects in 2D structures. Thus, there is a pressing need for the development of novel structures. In this regard, Li *et al.* devised a hydrogen-bond reinforced superstructure to fabricate a robust cathode for high-performance AZIBs. The resulting $Mg_{0.9}Mn_3O_7 \cdot 2.7H_2O$ material exhibits a distinctive motif characterized by a pinned Mg–Mn–Mg dumbbell configuration and interstratified hydrogen bonds, contributing to reduced migration and dissolution of Mn species as well as quasi-zero-strain behaviour.[93] Furthermore, the simultaneous co-confinement of multiple cations leads to enhanced structural integrity and cycling stability, attributed to the synergistic pillaring effect of multiple cations.[94]

NH_4^+, being one of the extensively investigated non-metallic cations, finds widespread application in layered vanadium and manganese oxides. Compared to metallic cations, NH_4^+ exhibits greater effectiveness in expanding the interlayer spacing of V_2O_5 owing to its larger ionic radius.[95] Furthermore, pre-intercalated NH_4^+ forms N–H···O bonds with the top and bottom layers of V_2O_5, acting as pillars that provide structural support to sustain the bilayers and prevent structural collapse during repeated ion de/intercalation processes.[96] The NH_4^+ pre-intercalated $V_2O_5 \cdot nH_2O$,[97] $(NH_4)_2V_4O_9$,[98] $NH_4V_4O_{10}$,[96] and $(NH_4)_2V_{10}O_{25} \cdot 8H_2O$[99] cathodes demonstrate an expanded tunnel structure, exceptional conductivity, and superior structural stability for aqueous ZIBs. These cathodes exhibit fast Zn^{2+} diffusion and excellent performance. Recently, NH_4^+ ions have been intercalated into layered MnO_2, resulting in the enlargement of the interlayer space and the formation of hydrogen bonds. These modifications contribute to enhanced structural robustness and fast reaction kinetics (Fig. 5c).[100]

Intercalation of organic molecules is assumed to expand the interlayer space and reinforce a layered structure. The PANI-intercalated MnO_2 nanolayers exhibit remarkable cycling stability and charge/discharge depth. It has been demonstrated that the PANI-reinforced layered structure of MnO_2 can effectively mitigate the hydrated H^+/Zn^{2+} insertion induced phase transformation and subsequent structural collapse, which is crucial for achieving a prolonged cycle life and high capacity.[101] Furthermore, it is found that the PANI layer serves a dual role in the (V_2O_{5-x})/polyaniline superlattice structure by acting as a spacer to expand interlayer spacing and as a conductive capacity contributor.[102] The expanded interlayer spacing is beneficial for achieving a zero-strain behaviour of Zn^{2+} during the de/intercalation process. As depicted in Fig. 5d, Wang *et al.* implemented a scalable water-bath strategy to precisely modulate the (001) spacing of bulk V_2O_5 from its initial value of 4.37 Å to 14.2 Å. This methodology involved the introduction of intercalated PANI molecules as pillars within the V_2O_5 interlayer, thereby resulting in the creation of abundant storage sites and enhanced diffusivities of hydrated Zn^{2+}. Remarkably, the PANI-intercalated V_2O_5 architecture exhibits zero-strain behavior even after undergoing multiple Zn^{2+} de/intercalation cycles.[103] It is important to note that the expansion of interlayer spacing may not be universally observed upon the insertion of organic species. In the $VOPO_4 \cdot H_2O$ cathode, the peak positions of all "*l*"-dependent *hkl* planes shift towards higher 2θ angles following polypyrrole (PPy) intercalation, indicating a contraction in the unit cell dimension along the *c*-axis. This contraction in the "*c*" unit cell length leads to a reduction in the spacing between the $VOPO_4$ layers from 7.43 Å (in $VOPO_4 \cdot 2H_2O$) to 6.72 Å, as calculated using the (001) planes. However, the PPy-intercalated $VOPO_4 \cdot H_2O$ exhibits significantly improved cycling stability.[104] Therefore, while a larger interlayer spacing facilitates Zn^{2+} ion de/intercalation, maintaining high structural stability is equally crucial for achieving prolonged cycling.

The co-intercalation of organic and inorganic species in layered cathodes is hypothesized to exhibit a synergistic mechanism, contributing to the enhancement of Zn^{2+} ion storage capacity. Bin *et al.* designed a layered PEDOT–$NH_4V_3O_8$ composite through a simple reflux method. The incorporation of conductive PEDOT resulted in an increased interlayer spacing of 10.8 Å compared to 7.8 Å for pure $NH_4V_3O_8$. The presence of oxygen vacancies and the enlarged interlayer spacing, facilitated by the polymer assistance, were found to contribute to the enhanced electrochemical performance.[105] Furthermore, the robustness of organic molecules within the

interlayers is crucial for achieving prolonged cycling stability during repeated Zn^{2+} de/intercalation processes. Wan *et al.* developed a universal compensation strategy by introducing polar organic molecules into the interlayer of Al^{3+} ion pre-intercalated $V_2O_5 \cdot nH_2O$ cathodes. The high-polarity groups in the organic molecules exhibit strong electrostatic attraction with pre-intercalated Al^{3+}, anchoring the organic molecules within the interlayer. Additionally, the low-polarity groups impart weak interaction with Zn^{2+} during cycling, enabling reversible Zn^{2+} transfer.[106]

3.2 Defect structure regulation

Creating and manipulating defect structures in electrode materials yields several beneficial effects. Firstly, the presence of defect structures generates additional active sites within the material host, thereby enhancing its capability for ion storage. Secondly, the controlled defect structure enables the modulation of the conductivity of electrode materials, which positively impacts charge transfer kinetics. Additionally, regulating the defect structure of electrode materials optimizes their crystal structure or structural symmetry, resulting in improved stability of the overall structure. In the field of materials science, defects commonly refer to vacancies, which can be primarily categorized as anion vacancies and cation vacancies, as outlined below.

Among the defects in cathode materials for AZIBs, anion vacancies have received significant attention. Oxygen vacancies, in particular, are commonly observed in vanadium and manganese oxides. Ye *et al.* have successfully obtained oxygen vacancy-enriched V_2O_5 structures through a low-temperature calcination process.[107] Density functional theory (DFT) calculations indicate that the presence of oxygen vacancies reduces the diffusion barriers for Zn^{2+} ions within the cathode host and weakens the interaction between Zn and O atoms. These effects significantly contribute to the outstanding electrochemical performance observed (Fig. 6a). Wu *et al.* quantified the Zn^{2+} migration coefficient in oxygen vacancy-enriched $VOP_4 \cdot 2H_2O$ using the galvanostatic intermittent titration technique. The results indicated a six-order-of-magnitude increase in the materials with oxygen vacancies compared to the bulk counterpart. Simultaneously, DFT simulations indicated a significantly enhanced electron conductivity, a reduced bandgap, and an ultralow diffusion barrier, all attributed to the presence of oxygen vacancies.[108] Furthermore, the presence of oxygen vacancies in MnO_2 materials facilitates a more reversible adsorption/desorption process for Zn^{2+}. Oxygen vacancies in its structure contribute to an enhanced storage capability for Zn^{2+} due to the reduced number of electrons required for Zn–O bonding and the increased incorporation of valence electrons into the delocalized electron cloud of the material.[109]

Cation vacancies are believed to offer additional space for accommodating Zn^{2+} ions while also contributing to high structural stability. Zhao *et al.* reported a novel topological semimetal cathode, $Co_3Sn_2S_2$, and demonstrated structural regulation by introducing Sn vacancies.[110] The presence of Sn vacancies resulted in the creation of additional Zn^{2+} transfer channels and active sites, thereby promoting charge-storage kinetics and enhancing the Zn^{2+} storage capability. It is noteworthy that the concentration of Sn vacancies requires careful and controlled adjustment to attain optimal performance (Fig. 6b). Moreover, the presence of Al cation vacancies in MnO_2 cathodes, generated through an electrochemical oxidation process, leads to the creation of additional diffusion channels for Zn^{2+} ion storage. Simultaneously, the available Al atoms effectively suppress the Jahn–Teller distortion of the MnO_6 octahedron during cycling.[111] It appears that electrochemical oxidation is conducive to introducing vacancies. An electrochemical method was reported to activate MnO by inducing Mn defects. The resulting $Mn_{0.61}\square_{0.39}O$ structure provides more accessible pathways for the diffusion of Zn^{2+} ions during the charge/discharge process, thereby enhancing the cycling capability.[112]

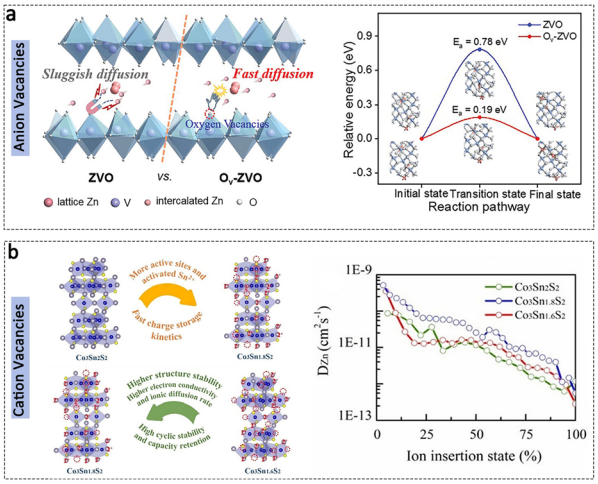

Fig. 6 Defect structure regulation. (a) Schematic illustration of the advantages of the anion vacancies of oxygen in the V_2O_5 electrode, and the diffusion barrier of Zn^{2+} migration in two electrodes. Adapted from ref. 107, copyright 2023, Wiley-VCH. (b) Advantages of $Co_3Sn_{1.8}S_2$ with appropriate concentration of Sn vacancies compared with $Co_3Sn_2S_2$ and $Co_3Sn_{1.6}S_2$; Co (blue ball), Sn (grey ball), S (yellow ball), Sn vacancy (dotted line circle), and the chemical diffusion coefficients for Zn^{2+} of three electrodes. Adapted from ref. 110, copyright 2021, Wiley-VCH.

3.3 Doping or compositing regulation

In addition to the presence of vacancies, the introduction of a dopant or heterogeneous atoms composed of other species can effectively regulate the crystal and electronic structure in materials. Doping strategies, such as cation doping and anion doping, enable the optimization of the intrinsic electronic structure of electrode materials, leading to enhanced conductivity and improved structural stability. Additionally, the design of compositions not only enhances the stability of cathode materials but also promotes the formation of a heterogeneous interface layer that facilitates electron transfer. These compositions typically encompass both organic/inorganic and inorganic/inorganic composites.

Doping heterogeneous atoms to replace the original atom sites induces changes in the structure and imparts the materials with new properties. Firstly, cation atom doping is used to optimize the electronic structure and improve the structural stability of the cathode materials in AZIBs. So far, some atoms have been introduced into the cathode materials, including V atoms for MnO_2,[113] Co atoms for MnO_2,[114] Ni atoms for V_6O_{13},[115] Mn atoms for VO_2,[116] Cu/Zn co-doping for PBAs, and so on.[117] The dissolution of Mn-based materials in the form of Mn^{2+} can be attributed to the Jahn–Teller (J–T) distortion arising from the disproportionation of Mn^{3+}. It can be inferred that the regulation of the degree of overlap between the atomic orbitals of Mn and O substantially alters the interaction of Mn–O bonds, consequently resulting in modifications to the electronic structure.[19] Therefore, doping heterogeneous atoms onto Mn-based-oxides can promote electronic rearrangement on the Mn–O bond. For instance, a NiMn-layered double hydroxide-derived Ni-doped Mn_2O_3 has been developed to mitigate the dissolution of manganese. The introduction of Ni^{2+} ions effectively stabilizes the Mn–O bond in Mn_2O_3 by reducing the formation energy (Fig. 7a).[118] Moreover, bimetallic Ni/Fe co-doping enables more effective optimization of the energy band structure and electronic state of manganese dioxide cathode materials.[119] Secondly, the introduction of dopant cation atoms into the host material enables the realization of high specific capacity through the utilization of the electrochemical redox reaction of the doped elements. Notably, the incorporation of Mn into $Na_3V_2(PO_4)_3$ to form $Na_4VMn(PO_4)_3$ has been observed to result in a significant enhancement in both capacity and working voltage. The electrochemical process for Zn-ion storage in $Na_4VMn(PO_4)_3$ has revealed a two-step electron transfer mechanism involving the V^{4+}/V^{3+} and Mn^{3+}/Mn^{2+} redox couples.[120]

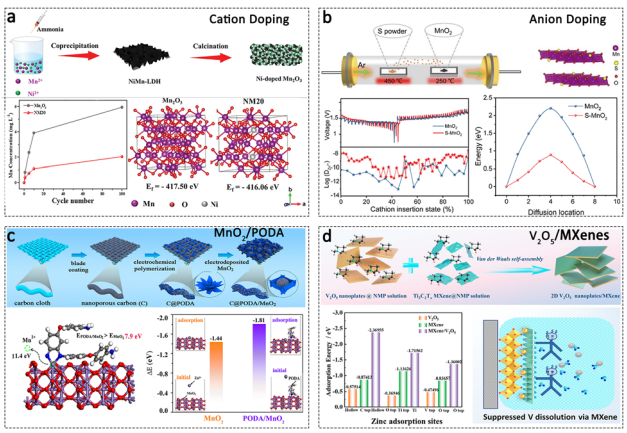

Fig. 7 Doping or compositing regulation. (a) Cation doping: Ni-doped Mn_2O_3 cathode. Adapted from ref. 118, copyright 2021, Wiley-VCH GmbH. (b) Anion doping: S-doped MnO_2 cathode. Adapted from ref. 122, copyright 2022, Elsevier B.V. (c) Organic/inorganic composites: MnO_2/PODA cathode. Adapted from ref. 123, copyright 2022, Wiley-VCH. (d) Inorganic/inorganic composites: V_2O_5/MXene cathode. Adapted from ref. 124, copyright 2022, American Chemical Society.

Anion doping is also an effective approach for regulating the electronic state and crystal structure. Nitrogen-doped ε-MnO_2 (MnO_2@N) has been synthesized through electrochemical deposition and subsequent heat treatment under a nitrogen atmosphere. The introduction of nitrogen doping results in an increase in oxygen vacancies, thereby enhancing the conductivity of the MnO_2@N cathode. Additionally, the presence of Mn–N bonds in MnO_2@N contributes to the improved electrochemical stability of the MnO_2@N cathode.[121] Similarly, sulfur-doped MnO_2 has been proposed for high-performance AZIBs. The research findings indicate that the incorporation of sulfur atoms into oxygen sites, characterized by lower electronegativity, can enhance the intrinsic electronic conductivity of MnO_2 and weaken the electrostatic interactions with multivalent Zn^{2+} cations (Fig. 7b).[122]

The electrochemical performance can be enhanced by combining two or more materials to form heterogeneous structures. One widely studied approach involves the combination of common cathode materials with carbon-based materials. Due to the high conductivity of carbon-based materials, these compositions exhibit excellent electronic transfer properties and remarkable electrolyte permeability. Typically, these compositions are assembled through physical adsorption, while novel composition structures with chemical interactions or intriguing properties are actively pursued. The interfacial design of a hybrid electrode with a unique bonding interface can not only achieve a stable material host but also provide new types of functionalities. Zhao *et al.* fabricated a novel hybrid cathode consisting of poly(4,4′-oxybisbenzenamine)/MnO_2 (referred to as C@PODA/MnO_2) through a two-step electrodeposition approach. The C=N groups present in the organic PODA component provide additional active sites for Zn^{2+} storage. Significantly, the newly formed Mn–N interfacial bonds effectively facilitate ion diffusion and inhibit Mn atom dissolution, enhancing the redox kinetics and structural integrity of MnO_2 (Fig. 7c).[123] Moreover, by combining various new inorganic materials with common cathode materials, multiple functionalities can be achieved. Liu *et al.* utilized a van der Waals self-assembly strategy to design an MXene layer on vanadium oxide materials (VPMX), which provides several advantages. Firstly, it preserves the structural integrity of the cathode surface and suppresses vanadium dissolution. Secondly, the heterointerface between V_2O_5 and MXenes facilitates enhanced electrochemical kinetics of the host material. Lastly, the presence of lubricating water molecules in the VPMX cathode diminishes electrostatic repulsion among the host layers, thereby promoting interfacial Zn^{2+} diffusion (Fig. 7d).[124] Recently, a ZnOTf-LDH (Zinc Triflate-Layered Double Hydroxide) artificial cathode–electrolyte interlayer was designed on the surface of the V_6O_{13} cathode. This artificial CEI acts as a barrier, repelling H_2O and blocking the migration of VO^{2+} and VO^{2+} species, while facilitating the transport of Zn^{2+} ions. Consequently, the undesired dissolution of V ions is effectively suppressed, and stable cycling performance was achieved over 200 cycles even at a low current density of 200 mA g^{-1}.[125]

3.4 Electrolyte regulation

Electrolytes function as the crucial link between the cathode and anode, and their properties significantly influence the reversibility of both electrodes.[126] It is assumed that electrolyte regulation can serve as an effective and feasible strategy, enabling simultaneous modulation of both the cathode and anode sides. For the cathode, the challenges related to dissolution, electrostatic interaction, and by-products can be significantly mitigated through the incorporation of electrolyte additives and the regulation of water content in the electrolyte.

On one hand, the incorporation of electrolyte additives aims to establish a dissolution equilibrium between the cathode and electrolyte. The addition of Mn^{2+} additives in the aqueous electrolyte has emerged as a widely acknowledged regulatory strategy to effectively retard the severe Mn dissolution from manganese oxide cathodes.[127] Pan *et al.* introduced $MnSO_4$ as an additive into a mild $ZnSO_4$ aqueous electrolyte, leading to the suppression of Mn dissolution in the MnO_2 nanofiber cathode.[63] Fig. 8a shows the cyclic voltammetry (CV) curves of Zn/MnO_2 batteries in electrolytes with and without $MnSO_4$. The observed similar redox behaviour suggests that the $MnSO_4$ additive did not significantly impact the redox reactions occurring in the MnO_2 electrodes. Nevertheless, the cycling properties are greatly enhanced with the electrolyte additive (Fig. 8b). Currently, in most AZIBs utilizing MnO_2 cathodes, $MnSO_4$ additives are incorporated into the electrolyte to suppress Mn dissolution, thereby achieving improved electrochemical performance. On the other hand, electrolyte additives contribute to the formation of a protective film on the cathode surface. In the $Zn(CF_3SO)_2$ electrolyte with the MnO_2 cathode, the $Mn(CF_3SO_3)_2$ additive has been observed to effectively suppress Mn dissolution and facilitate the formation of a uniform porous MnO_x nanosheet layer on the cathode surface. This layer plays a crucial role in maintaining the integrity of the electrode (Fig. 8c).[53] Similarly, in a $ZnMn_2O_4$ cathode, the introduction of $MnSO_4$ additive into the $ZnSO_4$ electrolyte also demonstrates a reversible electro-deposition/dissolution of a protective MnO_x layer on the cathode surface.[128] Additionally, the Na_2SO_4 and $MgSO_4$ additives have been found to enhance the stability of NaV_3O_8 and $Mg_xV_2O_5 \cdot nH_2O$ cathodes, respectively, by reducing the electrostatic interaction between the inserted ions and the cathode host.[41,129]

The utilization of water-in-salt electrolyte (WISE) showcases its ability to mitigate cathode material dissolution and suppress side reactions on the Zn anode, thereby enabling high capacity and stable cycling in AZIBs without the need for intricate surface coating, ion pre-intercalation, or defect engineering procedures. A 30 m $ZnCl_2$ WISE electrolyte is introduced to a MoO_3 nanobelt cathode, resulting in a significant enhancement in the stability of MoO_3 cathodes as compared to those operated in 3 m $ZnSO_4$ and $ZnCl_2$ electrolytes.[130] In the WISE electrolyte, Mo dissolution and its associated parasitic reactions were effectively suppressed due to the reduced presence of free H_2O (Fig. 8d). Similarly, the utilization of a 30 m $ZnCl_2$ WISE significantly mitigates the capacity fading issue, enabling unparalleled performance of a Zn battery cathode composed of $Ca_{0.2}V_2O_5 \cdot 0.8H_2O$.[131] Although a decrease in water content has the potential to enhance the stability of the cathode material in AZIBs, the presence of water is indispensable for the insertion and extraction of H^+ and Zn^{2+} ions, which is essential for achieving both high capacity and prolonged lifespan. Chen *et al.* developed an asymmetric electrolyte system by integrating an inorganic solid-state electrolyte with a hydrogel electrolyte. The former component facilitates the highly reversible Zn metal anode, while the latter component enables the chemistry involving H^+ and Zn^{2+} in the cathode (Fig. 8e).[132]

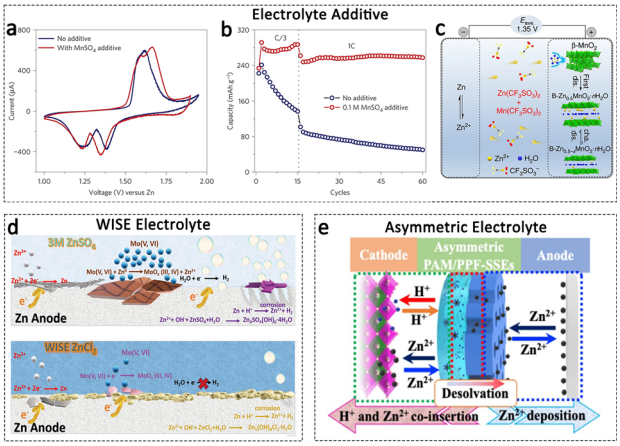

Fig. 8 Electrolyte regulation. (a) CV curves of MnO_2//Zn batteries with or without the $MnSO_4$ electrolyte additive; (b) cycling performance of MnO_2//Zn batteries with or without the $MnSO_4$ electrolyte additive. Adapted from ref. 63, copyright 2016, Springer Nature. (c) Schematic illustration of the rechargeable Zn–MnO_2 cell using a $CF_3SO_3^-$-based electrolyte. Adapted from ref. 53, copyright 2017, The Author(s). (d) Schematic showing the plausible reaction mechanisms at both MoO_3 cathode and Zn anode in 3 M $ZnSO_4$ and in 30 m $ZnCl_2$ WISE. Adapted from ref. 130, copyright 2021, Wiley-VCH. (e) Schematic illustration of an asymmetric electrolyte design. Adapted from ref. 132, copyright 2023, The Author(s).

4 Synchrotron radiation investigation

Synchrotron radiation light source is a pulsed light source characterized by its high luminosity, exceptional collimation, and precise controllability. Consequently, synchrotron radiation-based techniques serve as robust methodologies for probing regulated structures of the cathode materials for AZIBs. This section provides a comprehensive discussion on synchrotron radiation techniques employed for investigating the structural properties of cathode materials, including synchrotron radiation diffraction (SRXRD), X-ray absorption spectra (XAS), and other methodologies. Significantly, the utilization of *in situ* synchrotron radiation techniques plays a crucial role in unravelling the dynamic evolutionary processes of the electrode structures in AZIBs.

4.1 Synchrotron radiation X-ray diffraction (SRXRD)

X-ray diffraction analysis is employed for the examination of crystalline or partially crystalline materials. Synchrotron

radiation X-ray diffraction (SRXRD) shares similar principles with conventional laboratory XRD and serves as a powerful technique for elucidating crystallographic information, including lattice parameters, phases, and microstructural details. SRXRD differs from conventional laboratory XRD primarily in the utilization of synchrotron radiation as the X-ray source for diffraction, whereas conventional XRD relies on K_α radiation from Cu or Mo targets.[22] The high collimation and brilliance of synchrotron radiation make SRXRD a powerful tool for investigating material microstructures at a microscopic level. The resolution of SRXRD patterns can reach 0.002°, which is approximately two orders of magnitude higher than that achieved with laboratory sources. This enables the study of complex structures and the determination of phase composition, lattice parameters, residual stresses, and other valuable information through refined data analysis.

SRXRD allows for the acquisition of high signal-to-noise ratio diffraction data in a shorter time. Therefore, the SRXRD technique exhibits the capability of acquiring high-quality data during battery operation, enabling the analysis of the microstructural evolution process of cathode materials for AZIBs. For example, Pang *et al.* have utilized the SRXRD technique to investigate the reversible de/insertion of Zn^{2+} from/into the VO_2(B) cathode.[133] Through detailed Rietveld refinement, the changes in structural parameters and phase ratios of Zn_xVO_2 and the by-product $(Zn(OH)_2)_3(ZnSO_4)\cdot 5H_2O$ during the electrochemical reaction of Zn^{2+} were elucidated. The results reveal that the discharge process involved solid-solution insertion of Zn^{2+} into the VO_2(B) electrode, resulting in an 11.47% volume expansion. During the subsequent charge process, the lattice parameters of the Zn_xVO_2 phase returned to their initial values, indicating the structural reversibility of the active material. The lattice parameters of the by-product remained unchanged during discharge, but its relative amount increased, reaching 63 wt% of the entire electrode at the end of discharge, and subsequently decreased until nearly disappearing at the end of charge (Fig. 9a). Identically, high-resolution SRXRD data, in conjunction with Rietveld refinement, were used to establish a precise correlation between the alterations in the crystal structure of $Na_3V_2(PO_4)_3$ for the intercalation process involving Na^+ and Zn^{2+}. The findings elucidate that the initial charging of $Na_3V_2(PO_4)_3$ leads to the extraction of Na^+, resulting in the formation of an Na^+-depleted phase corresponding to $NaV_2(PO_4)_3$. Subsequent discharge predominantly involves the intercalation of Na^+ ions, followed by the intercalation of Zn^{2+}, leading to the formation of $Na_3V_2(PO_4)_3$ and $Zn_xNaV_2(PO_4)_3$, respectively.[134]

The SRXRD analysis is limited in its ability to extract detailed structural information from disordered materials, as it typically yields broadened diffraction peaks or background signals. Hence, the incorporation of total scattering analysis becomes imperative. By employing normalization and Fourier transformation techniques on both the Bragg diffraction peaks and diffuse scattering, this combined approach enables the determination of atomic order information over long-range distances and also provides insights into the short-range structural characteristics of the material.[135] For example, Shan *et al.* have utilized SRXRD to confirm the complete conversion of V_2O_5 to

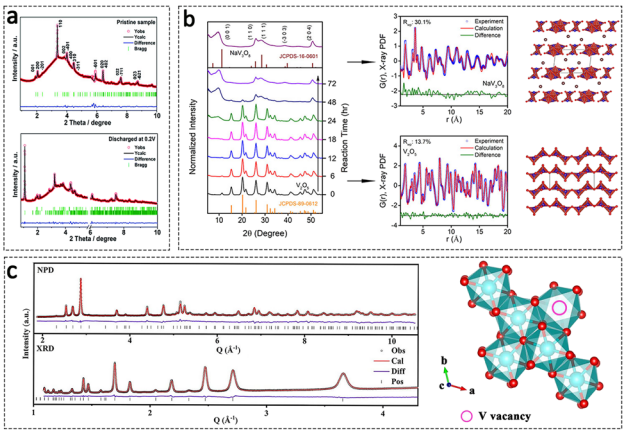

Fig. 9 SRXRD technique for the study of cathode materials in AZIBs. (a) The SRXRD data for VO_2(B) cathodes in the pristine and discharged states, respectively (λ = 0.2072 Å). Adapted from ref. 133, copyright 2020, The Royal Society of Chemistry. (b) XRD patterns illustrating the phase evolution during synthesis (the synchrotron-based wavelength of 0.166 Å converted to the Cu Kα), along with X-ray PDFs and fitted crystal structures of NaV_3O_8 and V_2O_5. Adapted from ref. 136, copyright 2020, American Chemical Society. (c) XRD and NPD patterns of the V_2O_3 cathode materials with V vacancies. Adapted from ref. 137, copyright 2021, The Author(s).

NaV_3O_8.[136] The diffraction pattern of the fully converted product, as depicted in Fig. 9b, exhibited indexing to monoclinic NaV_3O_8 with an enlarged interlayer spacing of 9.35 Å. Notably, NaV_3O_8 displayed broadened and asymmetric diffraction peaks, indicating a highly disordered nature. Hence, X-ray total scattering and PDF fitting were employed to gain insights into the detailed structures. The findings revealed that V_2O_5 possessed a well-defined orthorhombic layered structure with continuous connections between the VO_5 pyramid units. In contrast, NaV_3O_8 consisted of a double-sheet V_3O_8 framework in the *a*–*b* plane, comprising VO_5 octahedra and VO_6 square pyramid units. NaV_3O_8 did not exhibit a composition of continuous V–O polyhedra; instead, only a fraction of the polyhedra was connected through edge-sharing.

In summary, synchrotron X-ray diffraction (SRXRD) offers a highly advanced analytical approach with specific wavelength, extremely high energy, and exceptional spatiotemporal resolution, enabling comprehensive investigations into the structural properties and evolution processes of electrochemical energy storage materials. However, X-ray analysis lacks sensitivity towards light elements such as O and N. Therefore, it is crucial to combine X-ray-based techniques with complementary methods for accurate quantification of the structural properties of analytical materials. In our previous research, we employed neutron and X-ray powder diffraction measurements to quantify the presence of vanadium-defective clusters (up to 5.7%) in the V_2O_3 lattice (Fig. 9c).[137] Accurately quantifying and identifying the effects of defects through the integrated application of multiple spectroscopic techniques provide a deeper understanding for the advancement of rational design of cathodes with enhanced long-term stability for energy storage devices.

4.2 X-ray absorption spectra (XAS)

X-ray absorption spectroscopy (XAS) is a technique used to analyse the correlation between the incident photon energy and the X-ray absorption coefficient of the tested sample. XAS is capable of analysing a wide range of substances, including solids, liquids, and gases.[138] As mentioned above, X-ray diffraction characterization techniques are limited to examining crystalline materials. Nonetheless, researching amorphous materials or the conversion of crystals to non-crystalline states during operation is an ongoing and demanding topic in the field of AZIBs. Therefore, synchrotron radiation XAS offers a unique opportunity for investigating the local microstructure of the materials. According to the intensity of the incident X-ray, XAS can be divided into soft XAS (sXAS) and hard XAS (hXAS). sXAS primarily concentrates on the absorption process of incident photon energy below 2000 eV. It is utilized for the examination of K-edge absorption spectra, encompassing 1s → 2p electron transitions in light elements such as C, N, O, and F, as well as L-edge absorption spectra, which involve 2p → 3d electron transitions in transition metal elements such as V, Cr, and Mn. sXAS is capable of investigating the electronically unoccupied or occupied states of a wide range of elements commonly found in materials science. It plays a crucial role in the examination of chemical bonding information within materials. hXAS is predominantly employed for investigating the absorption process of specific atoms within the energy range of a few keV to tens of keV of incident photons. It is primarily focused on studying the K-edge absorption spectra, which involve 1s → 4p electronic transitions of transition metal atoms such as Ti, V, Mn, Zn, Nb, Mo, and others. XAFS (X-ray absorption fine structure) generally encompasses two components: X-ray absorption near-edge structure (XANES) within the range of 30–50 eV near the absorption edge, and extended X-ray absorption fine structure (EXAFS) within the range of 30–100 eV or even further beyond the absorption edge. XANES provides information on the average oxidation state, charge transfer, and unoccupied state density of the central atom, while EXAFS reveals details such as the type and coordination number of the surrounding atoms, the average bond length of neighbouring atoms, and the mean square disorder of adjacent atoms.[139]

sXAS is extensively employed for analysing the L-edge information of cations in AZIB cathode materials, thereby providing insights into the electronic and atomic orbital information. L-edge sXAS of transition metals provides a direct investigation of the 3d unoccupied states of the metal *via* dipole-allowed 2p-to-3d transitions. For instance, the Mn L_3-edge enables differentiation between the oxidation states of Mn^{4+} and Mn^{3+}. The observed peak dynamics in the Mn L-edge sXAS of a cation-deficient spinel $ZnMn_2O_4$ cathode provide clear evidence of electron transfer associated with the Mn^{3+}/Mn^{4+} redox couple. Additionally, the presence of tetravalent Mn correlates with the determined composition of $ZnMn_{1.86}Y_{0.14}O_4$ (Y representing a vacancy).[140] Interlayer engineering is recognized as an effective strategy for enhancing the performance of layered materials in AZIBs. sXAS offers valuable insights into the mechanism of intercalation agents and their functioning.

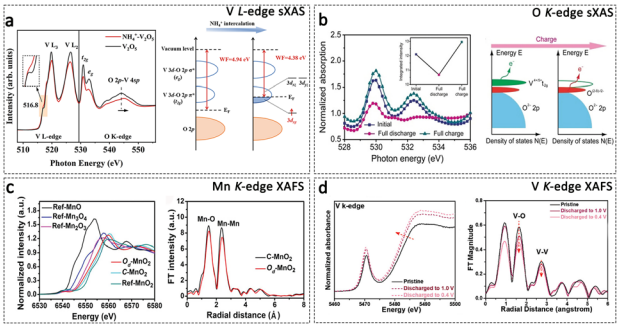

Fig. 10 XAS technique for the study of cathode materials in AZIBs. (a) V L-edge sXAS spectra of NH_4^+–V_2O_5 and V_2O_5, and the schematic diagram of the electron transition in NH_4^+–V_2O_5. Adapted from ref. 141, copyright 2023, PNAS. (b) Oxygen SXAS spectra and diagram of energy *versus* density of states in $VOPO_4$ electrodes. Adapted from ref. 142, copyright 2019, Wiley-VCH. (c) Mn K-edge XAFS spectra of O_d-MnO_2 and C–MnO_2. Adapted from ref. 109, copyright 2019, Wiley-VCH. (d) V K-edge XAFS spectra of $H_{3.78}V_6O_{13}$ during discharging. Adapted from ref. 146, copyright 2023, Wiley-VCH.

Our group used sXAS measurements to gain an in-depth understanding of the atomic orbital variations of V atoms induced by NH_4^+ intercalants.[141] As illustrated in Fig. 10a, the peak observed at 516.8 eV in the pre-edge region corresponds to the V $3d_{xy}$ state, which represents the lowest unoccupied state in the V t_{2g} orbital. In NH_4^+–V_2O_5, the width of this peak is broadened, and its resonance is reduced compared to commercial V_2O_5. These observations indicate electronic transitions from NH_4^+ to the V $3d_{xy}$ state, thereby occupying the lowest conduction band.

Additionally, sXAS is a powerful technique that can be competent to study anionic atoms, such as O and N atoms. With the increased pursuit of higher energy density, attention had been transferred to simultaneous cationic and anionic redox reactions of the cathode material, which enables more capacity contributions. Wan *et al.* demonstrated the oxygen redox process in the $VOPO_4$ electrode by O K-edge sXAS.[142] As depicted in Fig. 10b, the integration of two peaks at 530.0 and 532.4 eV indicates the density of hole states above the Fermi level. In the fully charged state, the integrated intensity is higher than that of the initial state, which can be attributed to the oxidation of oxygen since the valence of vanadium and phosphorus remains unchanged. Moreover, Wang *et al.* devised an electrochemical oxidation strategy to accomplish the reversible redox of nonbonding oxygen in the $MnV_2O_6{\cdot}2H_2O$ cathode. The O K-edge sXAS provides compelling evidence to substantiate the reversibility of the oxygen redox process in the $MnV_2O_6{\cdot}2H_2O$ electrode.[143] Identically, the anionic redox reaction mechanism of N was also revealed through sXAS characterization. The N K-edge sXAS spectra indicate that the photon energy of 397.6 eV (N^{3-}–V) at the initial state changes to 398.1 eV (N^{2-}–V) in the fully discharged state and then recovered to 397.6 eV (N^{3-}–V) in the fully charged state.[144] An increasing amount of research will be conducted on the anionic redox reaction of cathode materials for AZIBs, with sXAS playing a pivotal role in elucidating their operational mechanisms.

Using the K-edge absorption spectra provided by hXAS enables the retrieval of both bulk-average chemical state and local microstructural information for cations in materials. As mentioned previously, the defect structure plays a crucial role in governing the electronic state and microstructure of materials. By utilizing the standard sample, we were able to discern the microstructure of the regulated materials. For instance, Xiong *et al.* utilized Mn K-edge XAFS spectra to investigate the presence of oxygen vacancies in the MnO_2 cathode (O_d-MnO_2). Fig. 10c demonstrates that the absorption energy edge position in O_d-MnO_2 lies between those of the standard MnO_2 and Mn_2O_3 samples, indicating an average Mn oxidation state between 3+ and 4+. However, the absorption edge position in O_d-MnO_2 is lower than in the as-prepared C–MnO_2 (which lacks oxygen vacancies), indicating a lower oxidation state in O_d-MnO_2 attributed to the presence of oxygen vacancies. In the corresponding EXAFS spectra, the relative intensity of the Mn–O peak in O_d-MnO_2 is lower than that in C–MnO_2, suggesting the presence of oxygen vacancies in O_d-MnO_2.[109] Similarly, the EXAFS spectrum was utilized to examine the presence of Mn vacancies in V_m-NMO materials ($NiMn_3O_7$ with vacancies). A reduction in the intensity of the Mn–Mn peak was observed, implying a decrease in the coordination number of Mn cations within the V_m-NMO materials.[145] Additionally, Cao *et al.* revealed the X-ray absorption chemistry of the $H_{3.78}V_6O_{13}$ cathode for AZIBs.[146] The results indicate that the V K-edge absorption experiences a downward shift in energy during the discharging process, indicating a reduction in the valence state of V. Furthermore, the FT-EXAFS spectra of $H_{3.78}V_6O_{13}$ revealed a great decrease in the length of V–O and V–V bonds after discharge to 0.4 V, which is attributed to the shorter chemical bond between V atoms in tetrahedral positions and O atoms compared to the octahedral position (Fig. 10d). In the field of sulfur and iodine cathodes, XAFS becomes one of the most important techniques to characterize the structure of conductive carriers for S and I_2, providing guidance on cathode material design.[147,148]

4.3 Other synchrotron radiation techniques

With the development of AZIBs, other synchrotron radiation techniques have also been applied to analyse the Zn^{2+} storage mechanism of the cathode materials. Among these techniques, synchrotron radiation X-ray fluorescence microscopy (XFM) is a reliable and non-destructive technique that allows for elemental mapping and identification of potential chemical elements.[24] This technique enables precise measurements through single-point analysis or 2D mapping, providing valuable insights into trace element analysis by decoding fluorescence spectra.[149] The dissolution of Mn in aqueous MnO_2/Zn batteries is a prevalent phenomenon, leading to the complexity of the Zn^{2+} storage mechanism. Using XFM measurement, it has been found that Mn dissolves from the cathode and is detected in the electrolyte as Mn ions upon discharge. In sharp contrast, the Mn intensity in the electrolyte is low in the fully charged state (Fig. 11a). These data provide direct evidence that Mn^{2+} dissolution–deposition is the primary charge storage mechanism.[150]

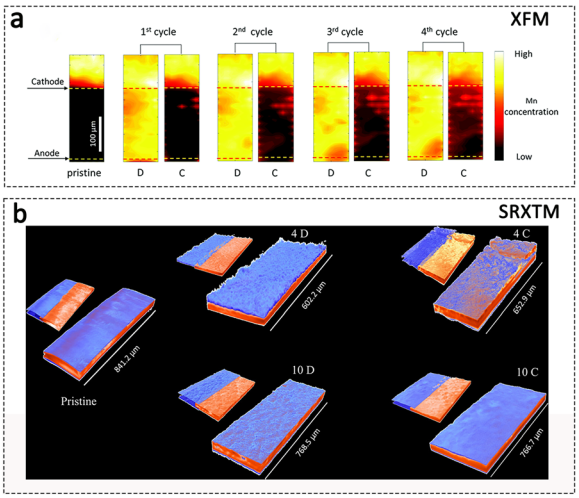

Fig. 11 Other synchrotron radiation techniques for the study of cathode materials in AZIBs. (a) Mn fluorescence maps in the fully discharged (D) and charged (C) states. Adapted from ref. 150, copyright 2020, The Royal Society of Chemistry. (b) SRXTM images of pristine, discharged and charged electrodes at the 4th and 10th cycles. The smaller figures adjacent to the electrodes represent the sectioned blue and red-colored phases in the respective cases. Adapted from ref. 152, copyright 2020 Wiley-VCH.

Synchrotron radiation X-ray tomographic microscopy (SRXTM) is utilized for direct visualization of the three-dimensional microstructure, elemental distribution, and content information of cathode materials in AZIBs. This technique utilizes absorption contrast based on variations in elemental composition, densities, and path lengths.[151] For example, Kumar *et al.* utilized SRXTM characterization to provide visual insights into the formation of new phases during cycling in the $FeVO_4$ cathode at submillimeter length scales, supporting the evidence for a conversion-type mechanism.[152] As shown in Fig. 11b, three electrodes, including pristine, discharged and charged electrodes at the 4th and 10th cycles, exhibit two regions of X-ray attenuating phases: high absorption for the deep material (colored in red) and low absorption for the surface material (colored in blue). The results indicate that the pristine electrode with a flat and uniform morphology results from the electrode fabrication process. After the 4th discharge, the electrode surface undergoes significant roughening, characterized by the formation of ridge/valley-like features indicative of material electrodeposition. In contrast, the electrode surface exhibits significant smoothening and regions of non-uniform X-ray attenuation after the 4th charge. This roughening/smoothening behavior continues through to the 10th charge/discharge cycle. The SRXTM technique gives a clear visual indication of the reversible phases forming at the micron scale and presents strong evidence for the conversion-type storage mechanism for AZIBs' cathode.

Additionally, synchrotron radiation photoelectron spectroscopy (SRPES) allows for obtaining element composition

information at different depths due to the tunable photon energy.[153] This capability facilitates the gradient detection of electrode/electrolyte interfaces. Furthermore, by selecting photon energies that correspond to higher ionization cross-sections for specific elements, a stronger detection signal can be achieved. Additionally, placing the incident photon energy in the ultraviolet range enables the acquisition of high-quality ultraviolet photoelectron spectroscopy (UPS) data, facilitating the analysis of the sample's work function and valence band structure. In our study, UPS measurements were performed to analyse the work function and valence band structure of NH_4^+ intercalated V_2O_5 electrodes. The results revealed a decrease in the work function from 4.94 to 4.38 eV upon NH_4^+ insertion, indicating the occupation of the V t_{2g} orbital by the intercalating NH_4^+ species.[141]

4.4 *In situ* synchrotron radiation technique

Leveraging the high brightness and collimation of synchrotron radiation light sources, the *in situ* synchrotron radiation techniques play a crucial role in enhancing the understanding of the dynamic structural evolution of cathode materials during Zn^{2+} chemistry. The design of cells for *in situ* experiments represents the primary focus of research, aiming to satisfy the X-ray path under the real electrochemical processes. Furthermore, it is imperative to avoid the use of components that are susceptible to corrosion in the aqueous electrolyte. For instance, the cell with a Be window that was employed in the organic cell in our previous study is not suitable.[154] We have employed coin cells with central trepans, and the trepans on both the anode and cathode were sealed using Kapton adhesive tape for the *in situ* experiment (Fig. 12a).[155] It is worth noting that a central trepanning operation should be conducted at the centre of the zinc wafer to mitigate the pronounced X-ray absorption of Zn. Moreover, any cell that satisfies both the requirements of *in situ* synchrotron radiation techniques and the ability to achieve genuine electrochemical reactions can be utilized for *in situ* experiments, like other home-made cells and pouch cells (Fig. 12b).[156]

The *in situ* SRXRD is the predominant technique used for monitoring the phase structure of cathode materials in AZIBs. Layered materials are widely regarded as suitable hosts for Zn^{2+} storage, as their interlayer spacing can undergo reversible de/intercalation of Zn^{2+}, leading to variations in the layer space. As described above, the interlayer engineering is an effective approach to enhance the structure robustness during cycling. Li *et al.* demonstrated the high reversibility of Zn^{2+} intercalation and extraction into/from the superlattice structure of vanadium oxide (V_2O_{5-x})/polyaniline using *in situ* SRXRD as experimental evidence (Fig. 13a).[102] However, it should be noted that not all pre-intercalated cathode materials exhibit interlayer expansion and contraction during cycling. Zhao *et al.* demonstrated through *in situ* SRXRD that NH_4^+ pre-intercalated $V_2O_5 \cdot nH_2O$ nanobelts undergo reversible solid-solution reactions and two-phase transitions during charge–discharge cycling, accompanied by the reversible formation and decomposition of a $ZnSO_4$-$Zn_3(OH)_6 \cdot 5H_2O$ by-product.[97] Furthermore, by employing *in situ* SRXRD characterization to investigate the evolution of phase structure, it is possible to analyse the types of embedded ions. Sun *et al.* discovered that the synthesized ultrathin Bi_2O_2Se nanosheets can efficiently activate stable proton storage in AZIBs, rather than large Zn^{2+} ions (Fig. 13b). *In situ* SRXRD confirms the energy storage mechanism involving a highly reversible process of proton insertion and extraction.[157] The energy storage mechanism of a Mn-based compound is complex. Wu *et al.* conducted *in situ* SRXRD to investigate the mechanism of aqueous Zn/a-MnO_2 batteries with $ZnSO_4$ electrolyte.[158] The results revealed the formation of a new phase, $Zn_4SO_4(OH)_6 \cdot 5H_2O$, during discharging, which subsequently disappeared during charging. This observation aligns with the prevailing

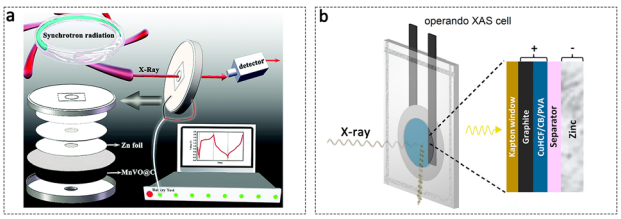

Fig. 12 X-ray *in situ* cells for the study of cathode materials in AZIBs. (a) Schematic diagram of the *operando* synchrotron radiation X-ray test cells and measurement environment. Adapted from ref. 155, copyright 2021, The Royal Society of Chemistry. (b) Schematic diagram of the XAS cell setup, consisting of a pouch cell with an X-ray transparent Kapton window. Adapted from ref. 156, copyright 2021, The Authors. Published by American Chemical Society.

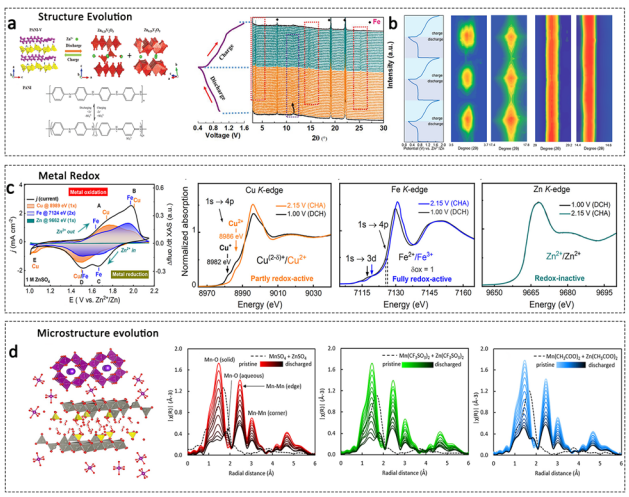

Fig. 13 *In situ* synchrotron radiation techniques for the study of cathode materials in AZIBs. (a) Structural evolution schematic diagram and *in situ* SRXRD patterns (λ = 0.6888 nm) of (V_2O_{5-x})/polyaniline cathode during cycling. Adapted from ref. 102, copyright 2020 Wiley-VCH. (b) *In situ* SXRD patterns of the Bi_2O_2Se cathode during cycling in AZIBs. Adapted from ref. 157, copyright 2021, American Chemical Society. (c) Potentiodynamic XAS-CV cycling experiments of Zn/CuHCF cell and the corresponding Cu, Fe, and Zn K-edge XANES spectra. Adapted from ref. 156, copyright 2021, The Authors. Published by the American Chemical Society. (d) Microstructure evolution schematic of the MnO_2 cathode and the corresponding Mn K-edge EXAFS spectra in $ZnSO_4$, $Zn(CF_3SO_3)$, and $Zn(CH_3COO)_2$ electrolytes, respectively. Adapted from ref. 159, copyright 2022, The Authors. Published by the American Chemical Society.

electrochemical process in AZIBs, where the reversible Mn dissolution–deposition reaction governs the electrochemistry.

In situ XAFS measurement is specifically tailored to capture the valence states and local structural evolution during the cycling process of AZIBs. The variation in valence states is a critical parameter that provides valuable insights, allowing a fine correlation between the electroactive species and the redox peaks in the cathode for AZIBs. Görlin *et al.* performed *in situ* XAFS to study the electroactive sites in the aqueous Zn/CuHCF cell.[156] *In situ* XAFS measurement used a pouch cell configuration with a Kapton window that allowed X-rays to pass through, and the fluorescence signal was monitored from the back side of the graphite current collector. Through the analysis of valence changes, it can be concluded that the Cu site exhibits partial redox activity, the Fe site shows full redox activity, while the Zn site is considered redox-inactive (Fig. 13c). Typically, the responses associated with Zn^{2+} insertion and extraction occur at localized regions within the cathode material. *In situ* XAFS allows for the monitoring of the overall evolution process of the local structure. *In situ* XAFS analysis was conducted to investigate the variations in electronic and local structures surrounding the V redox center in an NH_4^+ pre-intercalated vanadium cathode during electrochemical processes. In addition to the reversible reduction–oxidation of V during discharge–charge cycling, the *in situ* XAFS measurement revealed that the presence of inserted Zn^{2+} primarily influenced the nearest V–O shell structure while preserving the V–V shell structure almost unchanged, demonstrating its structural stability. Furthermore, *in situ* EXAFS analysis has the capability to quantitatively distinguish between different states of target atoms. Wu *et al.* introduced *operando* multiphase EXAFS analysis, enabling simultaneous characterization of both aqueous and solid phases involved in Mn redox reactions.[159] This methodology was successfully applied to multiple electrolytes ($ZnSO_4$, $Zn(CF_3SO_3)_2$, and $Zn(CH_3COO)_2$), revealing similar manganese coordination environments but quantitative differences in the distribution of Mn^{n+} species in the solid and solution phases (Fig. 13d). The *in situ* XAFS method provides a valuable means for the bulk characterization of poorly or non-crystalline, multiphase materials, including other polymorphs of Mn_xO_y, in complex environments.

Due to the rapid advancement of AZIBs, single synchrotron radiation technology is insufficient to meet the demands of multilevel and multiscale investigations of cathode materials. Throughout the entire electrochemical process, various changes occur in the phase, crystal structure, electron state, and morphology, resulting in a complex reaction pathway. Therefore, a combination of multiple synchrotron radiation techniques is desired to provide a comprehensive investigation of the cathode material. Recently, Kankanallu *et al.* employed multimodal synchrotron X-ray characterization to elucidate the dissolution–deposition reaction mechanism in aqueous Zn/MnO_2 batteries.[160] As shown in Fig. 14a, the *in situ* synchrotron X-ray diffraction revealed a crystalline-to-amorphous phase transition. The X-ray absorption spectra exhibited a gradual change, indicating the loss of crystalline MnO_2 species and an increase in the amorphous Zn–Mn complex. Scanning X-ray

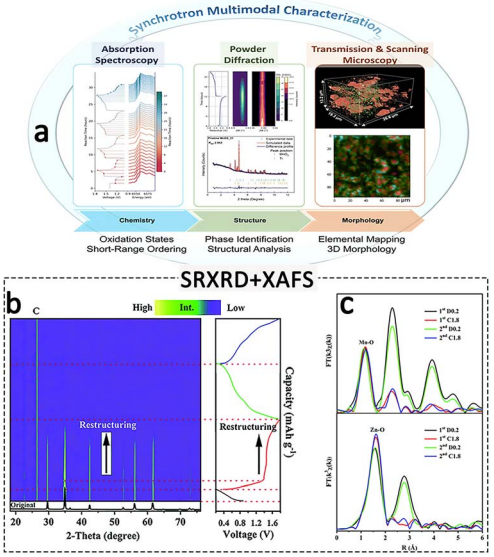

Fig. 14 Synchrotron multimodal characterization for the study of cathode materials in AZIBs. (a) Multi-modal X-ray synchrotron characterization of the energy storage mechanism of the MnO_2 cathode. Adapted from ref. 160, copyright 2023, The Royal Society of Chemistry. (b) *Operando* SXRD spectra of the MnV_2O_4@C cathode during cycling; (c) Mn and Zn EXAFS spectra of the MnV_2O_4@C cathode in different states. Adapted from ref. 155, copyright 2021, The Royal Society of Chemistry.

microscopy and full-field nano-tomography provided visual insights into the electrode morphology at different electrochemical states, enabling the spatial resolution of Zn- and Mn-containing phase formation. Our group utilized *in situ* SRXRD to constantly monitor the phase evolution of a spinel MnV_2O_4 cathode under operating conditions.[155] It was found that all the diffraction peaks became broadened after the initial charging to 1.8 V *vs.* Zn/Zn^{2+}, indicating a phase transition leading to the formation of an amorphous phase (Fig. 14b). Due to the limitations of SRXRD, which is primarily applicable to the study of long-range ordered materials, it is not feasible to gain a comprehensive understanding of the Zn^{2+} storage behaviour within an amorphous phase. Therefore, we further performed XAFS analysis to investigate the local structure evolution of the restructured electrode (Fig. 14c). Notably, XAFS measurements revealed an intriguing spatial migration of Mn ions. Specifically, when zinc ions are embedded, Mn ions occupy the tetrahedral site, whereas when zinc ions depart, Mn ions transition to the octahedral site. Accordingly, the significant buffer role of the mall amount of Mn ions was revealed.

5 Summary and outlook

In this review, we have firstly examined the structure, properties, and issues of typical cathode materials in AZIBs, including vanadium-based, manganese-based, Prussian blue analogue-based, as well as other materials. Subsequently, structure regulation strategies have been investigated to achieve improved electrochemical performance of cathode materials, with particular emphasis on the methods employed, their effects, and the

underlying mechanisms. Synchrotron radiation techniques are considered effective approaches for elucidating the structural characteristics of designed materials, enabling the identification of crystal structure, electronic structure, and local microstructure at multiple scales. Significantly, the structure dynamic evolution process of cathode materials, particularly with respect to phase structure, electronic state, and microstructure, can be visualized through the application of *in situ* synchrotron techniques, potentially in conjunction with multimodal techniques. In summary, significant advancements in capacity and stability of cathode materials for AZIBs have been achieved through structure regulation and synchrotron radiation investigation. However, substantial gaps remain between the current research status and practical application, indicating the necessity for persistent efforts and future endeavours in this field.

Future advancements for AZIBs' cathode materials are warranted in the following aspects:

(1) Precise regulation of the cathode material structure.

The interlayer engineering, defect structure, doping or compositing, and electrolyte regulation, along with other strategies, are believed to significantly influence the properties of cathode materials in AZIBs. One of the key challenges associated with these strategies is the achievement of precise regulation. It is expected that precise regulation can be achieved by establishing the structure–performance relationship through synchrotron radiation investigation. The types and concentrations of intercalating agents, defects, heterogeneous species, and electrolyte additives should be precisely controlled to attain an optimal formulation in the future.

(2) Research the operation mechanism under extreme conditions.

Despite significant efforts dedicated to the investigation of cathode materials under normal conditions, limited attention has been given to the exploration of the operational mechanisms under extreme conditions. Hence, it is imperative to conduct research on the microstructure evolution, interface chemistry, and ion transport behaviours of cathode materials for AZIBs under extreme conditions. Firstly, special attention should be given to the extreme conditions, including low or high temperature, high pressure, and vacuum environments. To enable the application of cathodes under extreme conditions, proper electrolyte regulation should be carefully tailored. Secondly, AZIBs have demonstrated remarkably high-rate performance.[161,162] However, it is still unclear whether H^+ or Zn^{2+} contributes dominantly under such high current densities. Based on the advantages of synchrotron light source, millisecond time-resolved XRD and XAFS, as well as other techniques are developed, making it possible to study the structural evolution of cathodes in AZIBs at ultra-high current densities. Furthermore, the practical application of AZIBs is hindered by their poor cycling performance at low currents.[9] Due to its tunable energy, high flux, and numerous other advantages, synchrotron-based X-ray techniques have also developed as an advanced non-destructive characterization method for detection of the electrode structure at ultra-low current density.

(3) Development of advanced synchrotron radiation techniques.

In order to achieve precise establishment of the structure–performance relationship of cathode materials, the utilization of synchrotron radiation techniques with high-resolution capabilities is desired. Usually, the evolution of an electrode material's structure begins with a local microregion quickly, where phenomena like dissolution and collapse are triggered by the shedding of individual atoms. Therefore, the development of high spatial and temporal resolution *in situ* probes is essential for analysing microregion reactions within electrode materials. In addition to utilizing advanced synchrotron radiation facilities, like fourth-generation synchrotron light sources, it is necessary to design *in situ* cells that can acquire high-quality data during real-time electrochemical reactions, as well as enable testing under specific extreme conditions, such as low or high temperature, high pressure, and gas environments. Meanwhile, the integration of synchrotron radiation techniques with complementary methods, such as microscopy, gas chromatography-mass spectrometry or data-driven machine learning approaches, holds great promise for enabling multi-dimensional studies of AZIBs. By combining diverse synchrotron radiation-based investigations with laboratory-based techniques, it becomes feasible to characterize the structure from the surface to the bulk, from the average to the local structure, and from micro to macro scales.

Data availability

We have no experimental or computational data associated with this article.

Author contributions

All authors contributed to the writing of the manuscript and approved the final version of the manuscript.

Conflicts of interest

There are no conflicts to declare.

Acknowledgements

This work was financially supported in part by the National Key R&D Program of China (2022YFA1605400, and 2022YFA1504104), the National Natural Science Foundation of China (12322515, U23A20121, 12225508, U2032113, and 22075264), the Youth Innovation Promotion Association of CAS (2022457), National Postdoctoral Program for Innovative Talents (BX20230346) and China Postdoctoral Science Foundation (2023M743365). We thank the Shanghai Synchrotron Radiation Facility (BL14W1, BL14B1, and SSRF), the Beijing Synchrotron Radiation Facility (1W1B, 4B7A, and BSRF), the Hefei Synchrotron Radiation Facility (BL11U, BL10B, MCD-A and MCD-B Soochow Beamline for Energy Materials at NSRL), and the USTC Center for Micro and Nanoscale Research and Fabrication for the help in characterization.

Notes and references

1 B. Dunn, H. Kamath and J.-M. Tarascon, Electrical Energy Storage for the Grid: A Battery of Choices, *Science*, 2011, **334**, 928–935.

2 G. Li, Y. Jin, M. W. Akram and X. Chen, Research and current status of the solar photovoltaic water pumping system – a review, *Renewable Sustainable Energy Rev.*, 2017, **79**, 440–458.

3 Z. Zhu, T. Jiang, M. Ali, Y. Meng, Y. Jin, Y. Cui and W. Chen, Rechargeable Batteries for Grid Scale Energy Storage, *Chem. Rev.*, 2022, **122**, 16610–16751.

4 L. E. Blanc, D. Kundu and L. F. Nazar, Scientific Challenges for the Implementation of Zn-Ion Batteries, *Joule*, 2020, **4**, 771–799.

5 N. Yabuuchi, K. Kubota, M. Dahbi and S. Komaba, Research Development on Sodium-Ion Batteries, *Chem. Rev.*, 2014, **114**, 11636–11682.

6 S. Wei, Z.-H. Qi, Y. Xia, S. Chen, C. Wang, Y. Wang, P. Zhang, K. Zhu, Y. Cao, X. Guo, X. Yang, Q. Cui, X. Liu, X. Wu and L. Song, Monolayer Thiol Engineered Covalent Interface toward Stable Zinc Metal Anode, *ACS Nano*, 2022, **16**, 21152–21162.

7 X. Yang, Q. Zhou, S. Wei, X. Guo, P. J. Chimtali, W. Xu, S. Chen, Y. Cao, P. Zhang, K. Zhu, H. Shou, Y. Wang, X. Wu, C. Wang and L. Song, Anion Additive Integrated Electric Double Layer and Solvation Shell for Aqueous Zinc Ion Battery, *Small Methods*, 2023, 2301115.

8 J. Ming, J. Guo, C. Xia, W. Wang and H. N. Alshareef, Zinc-ion batteries: materials, mechanisms, and applications, *Mater. Sci. Eng., R*, 2019, **135**, 58–84.

9 C. Li, S. Jin, L. A. Archer and L. F. Nazar, Toward practical aqueous zinc-ion batteries for electrochemical energy storage, *Joule*, 2022, **6**, 1733–1738.

10 C. Wang, S. Wei, S. Chen, D. Cao and L. Song, Delaminating Vanadium Carbides for Zinc-Ion Storage: Hydrate Precipitation and H^+/Zn^{2+} Co-Action Mechanism, *Small Methods*, 2019, **3**, 1900495.

11 G. Ma, Z. Ju, X. Xu, Y. Xu, Y. Sun, Y. Wang, G. Zhang, M. Cai, L. Pan and G. Yu, Enhancing organic cathodes of aqueous zinc-ion batteries via utilizing steric hindrance and electron cloud equalization, *Chem. Sci.*, 2023, **14**, 12589–12597.

12 T.-F. Yi, L. Qiu, J.-P. Qu, H. Liu, J.-H. Zhang and Y.-R. Zhu, Towards high-performance cathodes: design and energy storage mechanism of vanadium oxides-based materials for aqueous Zn-ion batteries, *Coord. Chem. Rev.*, 2021, **446**, 214124.

13 Y. Zhao, Y. Zhu and X. Zhang, Challenges and perspectives for manganese-based oxides for advanced aqueous zinc-ion batteries, *InfoMat*, 2020, **2**, 237–260.

14 G. Zampardi and F. La Mantia, Prussian blue analogues as aqueous Zn-ion batteries electrodes: current challenges and future perspectives, *Curr. Opin. Electrochem.*, 2020, **21**, 84–92.

15 C. Feng, X. Jiang, Q. Zhou, T. Li, Y. Zhao, Z. Niu, Y. Wu, H. Zhou, M. Wang, X. Zhang, M. Chen, L. Ni, G. Diao and Y. Wei, Recent advances in aqueous zinc–sulfur batteries: overcoming challenges for sustainable energy storage, *J. Mater. Chem. A*, 2023, **11**, 18029–18045.

16 X. Li, M. Li, Q. Yang, H. Li, H. Xu, Z. Chai, K. Chen, Z. Liu, Z. Tang, L. Ma, Z. Huang, B. Dong, X. Yin, Q. Huang and C. Zhi, Phase Transition Induced Unusual Electrochemical Performance of V_2CT_X MXene for Aqueous Zinc Hybrid-Ion Battery, *ACS Nano*, 2020, **14**, 541–551.

17 H. Liu, Z. Xin, B. Cao, B. Zhang, H. J. Fan and S. Guo, Versatile MXenes for Aqueous Zinc Batteries, *Adv. Sci.*, 2023, 2305806.

18 T. Sun, Z. Yi, W. Zhang, Q. Nian, H. J. Fan and Z. Tao, Dynamic Balance of Partial Charge for Small Organic Compound in Aqueous Zinc-Organic Battery, *Adv. Funct. Mater.*, 2023, **33**, 2306675.

19 A. Zhang, R. Zhao, Y. Wang, J. Yang, C. Wu and Y. Bai, Regulating the electronic structure of manganese-based materials to optimize the performance of zinc-ion batteries, *Energy Environ. Sci.*, 2023, **16**, 3240–3301.

20 M. Zhou, Y. Chen, G. Fang and S. Liang, Electrolyte/electrode interfacial electrochemical behaviors and optimization strategies in aqueous zinc-ion batteries, *Energy Storage Mater.*, 2022, **45**, 618–646.

21 P. S. Rahimabadi, M. Khodaei and K. R. Koswattage, Review on applications of synchrotron-based X-ray techniques in materials characterization, *X-Ray Spectrom.*, 2020, **49**, 348–373.

22 A. V. Llewellyn, A. Matruglio, D. J. L. Brett, R. Jervis and P. R. Shearing, Using In Situ Laboratory and Synchrotron-Based X-ray Diffraction for Lithium-Ion Batteries Characterization: A Review on Recent Developments, *Condens. Matter*, 2020, **5**, 75.

23 Z. Wu, W. Kong Pang, L. Chen, B. Johannessen and Z. Guo, In Situ Synchrotron X-Ray Absorption Spectroscopy Studies of Anode Materials for Rechargeable Batteries, *Batteries Supercaps*, 2021, **4**, 1547–1566.

24 L. Copeland-Hardin, T. Paunesku, J. S. Murley, J. Crentsil, O. Antipova, L. Li, E. Maxey, Q. Jin, D. Hooper, B. Lai, S. Chen and G. E. Woloschak, Proof of principle study: synchrotron X-ray fluorescence microscopy for identification of previously radioactive microparticles and elemental mapping of FFPE tissues, *Sci. Rep.*, 2023, **13**, 7806.

25 X. Xu, F. Xiong, J. Meng, X. Wang, C. Niu, Q. An and L. Mai, Vanadium-Based Nanomaterials: A Promising Family for Emerging Metal-Ion Batteries, *Adv. Funct. Mater.*, 2020, **30**, 1904398.

26 F. Wan and Z. Niu, Design Strategies for Vanadium-based Aqueous Zinc-Ion Batteries, *Angew. Chem., Int. Ed.*, 2019, **58**, 16358–16367.

27 N. Zhang, Y. Dong, M. Jia, X. Bian, Y. Wang, M. Qiu, J. Xu, Y. Liu, L. Jiao and F. Cheng, Rechargeable Aqueous Zn–V_2O_5 Battery with High Energy Density and Long Cycle Life, *ACS Energy Lett.*, 2018, **3**, 1366–1372.

28 X. Wang, Y. Li, S. Wang, F. Zhou, P. Das, C. Sun, S. Zheng and Z.-S. Wu, 2D Amorphous V_2O_5/Graphene Heterostructures for High-Safety Aqueous Zn-Ion Batteries with Unprecedented Capacity and Ultrahigh Rate Capability, *Adv. Energy Mater.*, 2020, **10**, 2000081.
29 J. Ding, Z. Du, L. Gu, B. Li, L. Wang, S. Wang, Y. Gong and S. Yang, Ultrafast Zn^{2+} Intercalation and Deintercalation in Vanadium Dioxide, *Adv. Mater.*, 2018, **30**, 1800762.
30 Z. Li, S. Ganapathy, Y. Xu, Z. Zhou, M. Sarilar and M. Wagemaker, Mechanistic Insight into the Electrochemical Performance of Zn/VO_2 Batteries with an Aqueous $ZnSO_4$ Electrolyte, *Adv. Energy Mater.*, 2019, **9**, 1900237.
31 W. Zhang, Y. Xiao, C. Zuo, W. Tang, G. Liu, S. Wang, W. Cai, S. Dong and P. Luo, Adjusting the Valence State of Vanadium in VO_2(B) by Extracting Oxygen Anions for High-Performance Aqueous Zinc-Ion Batteries, *ChemSusChem*, 2021, **14**, 971–978.
32 J. Lai, H. Zhu, X. Zhu, H. Koritala and Y. Wang, Interlayer-Expanded $V_6O_{13}\cdot nH_2O$ Architecture Constructed for an Advanced Rechargeable Aqueous Zinc-Ion Battery, *ACS Appl. Energy Mater.*, 2019, **2**, 1988–1996.
33 L. Shan, J. Zhou, W. Zhang, C. Xia, S. Guo, X. Ma, G. Fang, X. Wu and S. Liang, Highly Reversible Phase Transition Endows V_6O_{13} with Enhanced Performance as Aqueous Zinc-Ion Battery Cathode, *Energy Technol.*, 2019, **7**, 1900022.
34 L. Deng, H. Chen, J. Wu, Z. Yang, Y. Rong and Z. Fu, V_2O_3 as cathode of zinc ion battery with high stability and long cycling life, *Ionics*, 2021, **27**, 3393–3402.
35 D. Zhao, X. Pu, S. Tang, M. Ding, Y. Zeng, Y. Cao and Z. Chen, δ-VOPO4 as a high-voltage cathode material for aqueous zinc-ion batteries, *Chem. Sci.*, 2023, **14**, 8206–8213.
36 Z. Jian, Y.-S. Hu, X. Ji and W. Chen, NASICON-Structured Materials for Energy Storage, *Adv. Mater.*, 2017, **29**, 1601925.
37 G. Li, Z. Yang, Y. Jiang, C. Jin, W. Huang, X. Ding and Y. Huang, Towards polyvalent ion batteries: a zinc-ion battery based on NASICON structured $Na_3V_2(PO4)_3$, *Nano Energy*, 2016, **25**, 211–217.
38 P. He, M. Yan, G. Zhang, R. Sun, L. Chen, Q. An and L. Mai, Layered VS_2 Nanosheet-Based Aqueous Zn Ion Battery Cathode, *Adv. Energy Mater.*, 2017, **7**, 1601920.
39 Z. Wu, C. Lu, Y. Wang, L. Zhang, L. Jiang, W. Tian, C. Cai, Q. Gu, Z. Sun and L. Hu, Ultrathin VSe_2 Nanosheets with Fast Ion Diffusion and Robust Structural Stability for Rechargeable Zinc-Ion Battery Cathode, *Small*, 2020, **16**, 2000698.
40 D. Kundu, B. D. Adams, V. Duffort, S. H. Vajargah and L. F. Nazar, A high-capacity and long-life aqueous rechargeable zinc battery using a metal oxide intercalation cathode, *Nat. Energy*, 2016, **1**, 16119.
41 F. Wan, L. Zhang, X. Dai, X. Wang, Z. Niu and J. Chen, Aqueous rechargeable zinc/sodium vanadate batteries with enhanced performance from simultaneous insertion of dual carriers, *Nat. Commun.*, 2018, **9**, 1656.
42 M. H. Alfaruqi, V. Mathew, J. Song, S. Kim, S. Islam, D. T. Pham, J. Jo, S. Kim, J. P. Baboo, Z. Xiu, K.-S. Lee, Y.-K. Sun and J. Kim, Electrochemical Zinc Intercalation in Lithium Vanadium Oxide: A High-Capacity Zinc-Ion Battery Cathode, *Chem. Mater.*, 2017, **29**, 1684–1694.
43 C. Shen, X. Li, N. Li, K. Xie, J.-g. Wang, X. Liu and B. Wei, Graphene-Boosted, High-Performance Aqueous Zn-Ion Battery, *ACS Appl. Mater. Interfaces*, 2018, **10**, 25446–25453.
44 P. He, G. Zhang, X. Liao, M. Yan, X. Xu, Q. An, J. Liu and L. Mai, Sodium Ion Stabilized Vanadium Oxide Nanowire Cathode for High-Performance Zinc-Ion Batteries, *Adv. Energy Mater.*, 2018, **8**, 1702463.
45 P. He, Y. Quan, X. Xu, M. Yan, W. Yang, Q. An, L. He and L. Mai, High-Performance Aqueous Zinc–Ion Battery Based on Layered $H_2V_3O_8$ Nanowire Cathode, *Small*, 2017, **13**, 1702551.
46 N. Zhang, M. Jia, Y. Dong, Y. Wang, J. Xu, Y. Liu, L. Jiao and F. Cheng, Hydrated Layered Vanadium Oxide as a Highly Reversible Cathode for Rechargeable Aqueous Zinc Batteries, *Adv. Funct. Mater.*, 2019, **29**, 1807331.
47 W. Liu, L. Dong, B. Jiang, Y. Huang, X. Wang, C. Xu, Z. Kang, J. Mou and F. Kang, Layered vanadium oxides with proton and zinc ion insertion for zinc ion batteries, *Electrochim. Acta*, 2019, **320**, 134565.
48 X. Chen, L. Wang, H. Li, F. Cheng and J. Chen, Porous V_2O_5 nanofibers as cathode materials for rechargeable aqueous zinc-ion batteries, *J. Energy Chem.*, 2019, **38**, 20–25.
49 W. Li, K. Wang, S. Cheng and K. Jiang, A long-life aqueous Zn-ion battery based on $Na_3V_2(PO_4)_2F_3$ cathode, *Energy Storage Mater.*, 2018, **15**, 14–21.
50 M. E. Pam, D. Yan, J. Yu, D. Fang, L. Guo, X. L. Li, T. C. Li, X. Lu, L. K. Ang, R. Amal, Z. Han and H. Y. Yang, Microstructural Engineering of Cathode Materials for Advanced Zinc-Ion Aqueous Batteries, *Adv. Sci.*, 2021, **8**, 2002722.
51 M. H. Alfaruqi, J. Gim, S. Kim, J. Song, J. Jo, S. Kim, V. Mathew and J. Kim, Enhanced reversible divalent zinc storage in a structurally stable α-MnO_2 nanorod electrode, *J. Power Sources*, 2015, **288**, 320–327.
52 C. Wei, C. Xu, B. Li, H. Du and F. Kang, Preparation and characterization of manganese dioxides with nano-sized tunnel structures for zinc ion storage, *J. Phys. Chem. Solids*, 2012, **73**, 1487–1491.
53 N. Zhang, F. Cheng, J. Liu, L. Wang, X. Long, X. Liu, F. Li and J. Chen, Rechargeable aqueous zinc-manganese dioxide batteries with high energy and power densities, *Nat. Commun.*, 2017, **8**, 405.
54 M. H. Alfaruqi, V. Mathew, J. Gim, S. Kim, J. Song, J. P. Baboo, S. H. Choi and J. Kim, Electrochemically Induced Structural Transformation in a γ-MnO_2 Cathode of a High Capacity Zinc-Ion Battery System, *Chem. Mater.*, 2015, **27**, 3609–3620.
55 M. H. Alfaruqi, J. Gim, S. Kim, J. Song, D. T. Pham, J. Jo, Z. Xiu, V. Mathew and J. Kim, A layered δ-MnO_2 nanoflake cathode with high zinc-storage capacities for eco-friendly battery applications, *Electrochem. Commun.*, 2015, **60**, 121–125.
56 W. Sun, F. Wang, S. Hou, C. Yang, X. Fan, Z. Ma, T. Gao, F. Han, R. Hu, M. Zhu and C. Wang, Zn/MnO_2 Battery

Chemistry With H^+ and Zn^{2+} Coinsertion, *J. Am. Chem. Soc.*, 2017, **139**, 9775–9778.

57 J. Wang, J.-G. Wang, H. Liu, Z. You, C. Wei and F. Kang, Electrochemical activation of commercial MnO microsized particles for high-performance aqueous zinc-ion batteries, *J. Power Sources*, 2019, **438**, 226951.

58 B. Jiang, C. Xu, C. Wu, L. Dong, J. Li and F. Kang, Manganese Sesquioxide as Cathode Material for Multivalent Zinc Ion Battery with High Capacity and Long Cycle Life, *Electrochim. Acta*, 2017, **229**, 422–428.

59 Y. Guo, Y. Zhang and H. Lu, Manganese-based materials as cathode for rechargeable aqueous zinc-ion batteries, *Battery Energy*, 2022, **1**, 20210014.

60 J. Hao, J. Mou, J. Zhang, L. Dong, W. Liu, C. Xu and F. Kang, Electrochemically induced spinel-layered phase transition of Mn_3O_4 in high performance neutral aqueous rechargeable zinc battery, *Electrochim. Acta*, 2018, **259**, 170–178.

61 X. Chen, W. Li, Y. Xu, Z. Zeng, H. Tian, M. Velayutham, W. Shi, W. Li, C. Wang, D. Reed, V. V. Khramtsov, X. Li and X. Liu, Charging activation and desulfurization of MnS unlock the active sites and electrochemical reactivity for Zn-ion batteries, *Nano Energy*, 2020, **75**, 104869.

62 W. Shi, W. S. V. Lee and J. Xue, Recent Development of Mn-based Oxides as Zinc-Ion Battery Cathode, *ChemSusChem*, 2021, **14**, 1634–1658.

63 H. Pan, Y. Shao, P. Yan, Y. Cheng, K. S. Han, Z. Nie, C. Wang, J. Yang, X. Li, P. Bhattacharya, K. T. Mueller and J. Liu, Reversible aqueous zinc/manganese oxide energy storage from conversion reactions, *Nat. Energy*, 2016, **1**, 16039.

64 J. Cui, X. Wu, S. Yang, C. Li, F. Tang, J. Chen, Y. Chen, Y. Xiang, X. Wu and Z. He, Cryptomelane-Type KMn_8O_{16} as Potential Cathode Material - for Aqueous Zinc Ion Battery, *Front. Chem.*, 2018, **6**, 352.

65 X. Wu, Y. Xiang, Q. Peng, X. Wu, Y. Li, F. Tang, R. Song, Z. Liu, Z. He and X. Wu, Green-low-cost rechargeable aqueous zinc-ion batteries using hollow porous spinel $ZnMn_2O_4$ as the cathode material, *J. Mater. Chem. A*, 2017, **5**, 17990–17997.

66 S. Islam, M. H. Alfaruqi, V. Mathew, J. Song, S. Kim, S. Kim, J. Jo, J. P. Baboo, D. T. Pham, D. Y. Putro, Y.-K. Sun and J. Kim, Facile synthesis and the exploration of the zinc storage mechanism of β-MnO_2 nanorods with exposed (101) planes as a novel cathode material for high performance eco-friendly zinc-ion batteries, *J. Mater. Chem. A*, 2017, **5**, 23299–23309.

67 W. Zhao, Q. Kong, X. Wu, X. An, J. Zhang, X. Liu and W. Yao, ε-MnO_2@C cathode with high stability for aqueous zinc-ion batteries, *Appl. Surf. Sci.*, 2022, **605**, 154685.

68 Y. Zeng, X. F. Lu, S. L. Zhang, D. Luan, S. Li and X. W. Lou, Construction of Co–Mn Prussian Blue Analog Hollow Spheres for Efficient Aqueous Zn-ion Batteries, *Angew. Chem., Int. Ed.*, 2021, **60**, 22189–22194.

69 L. Chen, Q. An and L. Mai, Recent Advances and Prospects of Cathode Materials for Rechargeable Aqueous Zinc-Ion Batteries, *Adv. Mater. Interfaces*, 2019, **6**, 1900387.

70 L. Zhang, L. Chen, X. Zhou and Z. Liu, Towards High-Voltage Aqueous Metal-Ion Batteries Beyond 1.5 V: The Zinc/Zinc Hexacyanoferrate System, *Adv. Energy Mater.*, 2015, **5**, 1400930.

71 R. Trócoli and F. La Mantia, An Aqueous Zinc-Ion Battery Based on Copper Hexacyanoferrate, *ChemSusChem*, 2015, **8**, 481–485.

72 L. Zhang, L. Chen, X. Zhou and Z. Liu, Morphology-Dependent Electrochemical Performance of Zinc Hexacyanoferrate Cathode for Zinc-Ion Battery, *Sci. Rep.*, 2015, **5**, 18263.

73 D. Selvakumaran, A. Pan, S. Liang and G. Cao, A review on recent developments and challenges of cathode materials for rechargeable aqueous Zn-ion batteries, *J. Mater. Chem. A*, 2019, **7**, 18209–18236.

74 Y. Li, J. Zhao, Q. Hu, T. Hao, H. Cao, X. Huang, Y. Liu, Y. Zhang, D. Lin, Y. Tang and Y. Cai, Prussian blue analogs cathodes for aqueous zinc ion batteries, *Mater. Today Energy*, 2022, **29**, 101095.

75 J. Liu, Z. Shen and C.-Z. Lu, Research progress of Prussian blue and its analogues for cathode of aqueous zinc ion battery, *J. Mater. Chem. A*, 2024, **29**, 101095.

76 F. Wan, L. Zhang, X. Wang, S. Bi, Z. Niu and J. Chen, An Aqueous Rechargeable Zinc-Organic Battery with Hybrid Mechanism, *Adv. Funct. Mater.*, 2018, **28**, 1804975.

77 F. Ye, Q. Liu, H. Dong, K. Guan, Z. Chen, N. Ju and L. Hu, Organic Zinc-Ion Battery: Planar, π-Conjugated Quinone-Based Polymer Endows Ultrafast Ion Diffusion Kinetics, *Angew. Chem., Int. Ed.*, 2022, **61**, e202214244.

78 H. Furukawa, K. E. Cordova, M. O'Keeffe and O. M. Yaghi, The Chemistry and Applications of Metal-Organic Frameworks, *Science*, 2013, **341**, 1230444.

79 X. Pu, B. Jiang, X. Wang, W. Liu, L. Dong, F. Kang and C. Xu, High-Performance Aqueous Zinc-Ion Batteries Realized by MOF Materials, *Nano-Micro Lett.*, 2020, **12**, 152.

80 Z. Hu, Q. Liu, S.-L. Chou and S.-X. Dou, Advances and Challenges in Metal Sulfides/Selenides for Next-Generation Rechargeable Sodium-Ion Batteries, *Adv. Mater.*, 2017, **29**, 1700606.

81 X. Wang, Z. Zhang, B. Xi, W. Chen, Y. Jia, J. Feng and S. Xiong, Advances and Perspectives of Cathode Storage Chemistry in Aqueous Zinc-Ion Batteries, *ACS Nano*, 2021, **15**, 9244–9272.

82 L.-W. Luo, C. Zhang, X. Wu, C. Han, Y. Xu, X. Ji and J.-X. Jiang, A Zn–S aqueous primary battery with high energy and flat discharge plateau, *Chem. Commun.*, 2021, **57**, 9918–9921.

83 D. Lin and Y. Li, Recent Advances of Aqueous Rechargeable Zinc-Iodine Batteries: Challenges, Solutions, and Prospects, *Adv. Mater.*, 2022, **34**, 2108856.

84 H. Pan, B. Li, D. Mei, Z. Nie, Y. Shao, G. Li, X. S. Li, K. S. Han, K. T. Mueller, V. Sprenkle and J. Liu, Controlling Solid–Liquid Conversion Reactions for a Highly Reversible Aqueous Zinc–Iodine Battery, *ACS Energy Lett.*, 2017, **2**, 2674–2680.

85 X. Li, N. Li, Z. Huang, Z. Chen, G. Liang, Q. Yang, M. Li, Y. Zhao, L. Ma, B. Dong, Q. Huang, J. Fan and C. Zhi,

Enhanced Redox Kinetics and Duration of Aqueous I2/I− Conversion Chemistry by MXene Confinement, *Adv. Mater.*, 2021, **33**, 2006897.

86 M. Yan, P. He, Y. Chen, S. Wang, Q. Wei, K. Zhao, X. Xu, Q. An, Y. Shuang, Y. Shao, K. T. Mueller, L. Mai, J. Liu and J. Yang, Water-Lubricated Intercalation in $V_2O_5 \cdot nH_2O$ for High-Capacity and High-Rate Aqueous Rechargeable Zinc Batteries, *Adv. Mater.*, 2018, **30**, 1703725.

87 G. Zhang, T. Wu, H. Zhou, H. Jin, K. Liu, Y. Luo, H. Jiang, K. Huang, L. Huang and J. Zhou, Rich Alkali Ions Preintercalated Vanadium Oxides for Durable and Fast Zinc-Ion Storage, *ACS Energy Lett.*, 2021, **6**, 2111–2120.

88 C. Liu, Z. Neale, J. Zheng, X. Jia, J. Huang, M. Yan, M. Tian, M. Wang, J. Yang and G. Cao, Expanded hydrated vanadate for high-performance aqueous zinc-ion batteries, *Energy Environ. Sci.*, 2019, **12**, 2273–2285.

89 H. Geng, M. Cheng, B. Wang, Y. Yang, Y. Zhang and C. C. Li, Electronic Structure Regulation of Layered Vanadium Oxide via Interlayer Doping Strategy toward Superior High-Rate and Low-Temperature Zinc-Ion Batteries, *Adv. Funct. Mater.*, 2020, **30**, 1907684.

90 J. Li, K. McColl, X. Lu, S. Sathasivam, H. Dong, L. Kang, Z. Li, S. Zhao, A. G. Kafizas, R. Wang, D. J. L. Brett, P. R. Shearing, F. Corà, G. He, C. J. Carmalt and I. P. Parkin, Multi-Scale Investigations of δ-$Ni_{0.25}V_2O_5 \cdot nH_2O$ Cathode Materials in Aqueous Zinc-Ion Batteries, *Adv. Energy Mater.*, 2020, **10**, 2000058.

91 F. Ming, H. Liang, Y. Lei, S. Kandambeth, M. Eddaoudi and H. N. Alshareef, Layered $Mg_xV_2O_5 \cdot nH_2O$ as Cathode Material for High-Performance Aqueous Zinc Ion Batteries, *ACS Energy Lett.*, 2018, **3**, 2602–2609.

92 K. Zhu, T. Wu and K. Huang, A High Capacity Bilayer Cathode for Aqueous Zn-Ion Batteries, *ACS Nano*, 2019, **13**, 14447–14458.

93 J. Li, N. Luo, L. Kang, F. Zhao, Y. Jiao, T. J. Macdonald, M. Wang, I. P. Parkin, P. R. Shearing, D. J. L. Brett, G. Chai and G. He, Hydrogen-Bond Reinforced Superstructural Manganese Oxide As the Cathode for Ultra-Stable Aqueous Zinc Ion Batteries, *Adv. Energy Mater.*, 2022, **12**, 2201840.

94 Y. Liu, C. Lu, Y. Yang, W. Chen, F. Ye, H. Dong, Y. Wu, R. Ma and L. Hu, Multiple Cations Nanoconfinement in Ultrathin V2O5 Nanosheets Enables Ultrafast Ion Diffusion Kinetics Toward High-performance Zinc Ion Battery, *Adv. Mater.*, 2024, 2312982.

95 H. Jiang, Y. Zhang, Z. Pan, L. Xu, J. Zheng, Z. Gao, T. Hu and C. Meng, Facile hydrothermal synthesis and electrochemical properties of $(NH_4)_2V_{10}O_{25} \cdot 8H_2O$ nanobelts for high-performance aqueous zinc ion batteries, *Electrochim. Acta*, 2020, **332**, 135506.

96 B. Tang, J. Zhou, G. Fang, F. Liu, C. Zhu, C. Wang, A. Pan and S. Liang, Engineering the interplanar spacing of ammonium vanadates as a high-performance aqueous zinc-ion battery cathode, *J. Mater. Chem. A*, 2019, **7**, 940–945.

97 H. Zhao, Q. Fu, D. Yang, A. Sarapulova, Q. Pang, Y. Meng, L. Wei, H. Ehrenberg, Y. Wei, C. Wang and G. Chen, In Operando Synchrotron Studies of NH^{4+} Preintercalated $V_2O_5 \cdot nH_2O$ Nanobelts as the Cathode Material for Aqueous Rechargeable Zinc Batteries, *ACS Nano*, 2020, **14**, 11809–11820.

98 Y. Zhang, H. Jiang, L. Xu, Z. Gao and C. Meng, Ammonium Vanadium Oxide $[(NH_4)_2V_4O_9]$ Sheets for High Capacity Electrodes in Aqueous Zinc Ion Batteries, *ACS Appl. Energy Mater.*, 2019, **2**, 7861–7869.

99 J. Cao, D. Zhang, Y. Yue, X. Wang, T. Pakornchote, T. Bovornratanaraks, X. Zhang, Z.-S. Wu and J. Qin, Oxygen defect enriched $(NH_4)_2V_{10}O_{25} \cdot 8H_2O$ nanosheets for superior aqueous zinc-ion batteries, *Nano Energy*, 2021, **84**, 105876.

100 H. Yao, H. Yu, Y. Zheng, N. W. Li, S. Li, D. Luan, X. W. Lou and L. Yu, Pre-intercalation of Ammonium Ions in Layered δ-MnO_2 Nanosheets for High-Performance Aqueous Zinc-Ion Batteries, *Angew. Chem., Int. Ed.*, 2023, **62**, e202315257.

101 J. Huang, Z. Wang, M. Hou, X. Dong, Y. Liu, Y. Wang and Y. Xia, Polyaniline-intercalated manganese dioxide nanolayers as a high-performance cathode material for an aqueous zinc-ion battery, *Nat. Commun.*, 2018, **9**, 2906.

102 W. Li, C. Han, Q. Gu, S.-L. Chou, J.-Z. Wang, H.-K. Liu and S.-X. Dou, Electron Delocalization and Dissolution-Restraint in Vanadium Oxide Superlattices to Boost Electrochemical Performance of Aqueous Zinc-Ion Batteries, *Adv. Energy Mater.*, 2020, **10**, 2001852.

103 Z. Wang, X. Tang, S. Yuan, M. Bai, H. Wang, S. Liu, M. Zhang and Y. Ma, Engineering Vanadium Pentoxide Cathode for the Zero-Strain Cation Storage via a Scalable Intercalation-Polymerization Approach, *Adv. Funct. Mater.*, 2021, **31**, 2100164.

104 V. Verma, S. Kumar, W. Manalastas Jr, J. Zhao, R. Chua, S. Meng, P. Kidkhunthod and M. Srinivasan, Layered $VOPO_4$ as a Cathode Material for Rechargeable Zinc-Ion Battery: Effect of Polypyrrole Intercalation in the Host and Water Concentration in the Electrolyte, *ACS Appl. Energy Mater.*, 2019, **2**, 8667–8674.

105 D. Bin, W. Huo, Y. Yuan, J. Huang, Y. Liu, Y. Zhang, F. Dong, Y. Wang and Y. Xia, Organic-Inorganic-Induced Polymer Intercalation into Layered Composites for Aqueous Zinc-Ion Battery, *Chem*, 2020, **6**, 968–984.

106 F. Wan, Z. M. Hao, S. Wang, Y. X. Ni, J. C. Zhu, Z. W. Tie, S. S. Bi, Z. Q. Niu and J. Chen, A Universal Compensation Strategy to Anchor Polar Organic Molecules in Bilayered Hydrated Vanadates for Promoting Aqueous Zinc-Ion Storage, *Adv. Mater.*, 2021, **33**, 2102701.

107 J.-J. Ye, P.-H. Li, H.-R. Zhang, Z.-Y. Song, T. Fan, W. Zhang, J. Tian, T. Huang, Y. Qian, Z. Hou, N. Shpigel, L.-F. Chen and S. X. Dou, Manipulating Oxygen Vacancies to Spur Ion Kinetics in V_2O_5 Structures for Superior Aqueous Zinc-Ion Batteries, *Adv. Funct. Mater.*, 2023, **33**, 2305659.

108 Z. Wu, C. Lu, F. Ye, L. Zhang, L. Jiang, Q. Liu, H. Dong, Z. Sun and L. Hu, Bilayered $VOPO_4 \cdot 2H_2O$ Nanosheets with High-Concentration Oxygen Vacancies for High-Performance Aqueous Zinc-Ion Batteries, *Adv. Funct. Mater.*, 2021, **31**, 2106816.

109 T. Xiong, Z. G. Yu, H. Wu, Y. Du, Q. Xie, J. Chen, Y.-W. Zhang, S. J. Pennycook, W. S. V. Lee and J. Xue, Defect Engineering of Oxygen-Deficient Manganese Oxide to Achieve High-Performing Aqueous Zinc Ion Battery, *Adv. Energy Mater.*, 2019, **9**, 1803815.

110 Y. Zhao, Y. Zhu, F. Jiang, Y. Li, Y. Meng, Y. Guo, Q. Li, Z. Huang, S. Zhang, R. Zhang, J. C. Ho, Q. Zhang, W. Liu and C. Zhi, Vacancy Modulating $Co_3Sn_2S_2$ Topological Semimetal for Aqueous Zinc-Ion Batteries, *Angew. Chem.*, 2022, **134**, e202111826.

111 Y. Zhao, S. Zhang, Y. Zhang, J. Liang, L. Ren, H. J. Fan, W. Liu and X. Sun, Vacancy-rich Al-doped MnO_2 cathode breaks the trade-off between kinetics and stability for high-performance aqueous Zn-ion battery, *Energy Environ. Sci.*, 2023, **17**, 1279–1290.

112 C. Zhu, G. Fang, S. Liang, Z. Chen, Z. Wang, J. Ma, H. Wang, B. Tang, X. Zheng and J. Zhou, Electrochemically induced cationic defect in MnO intercalation cathode for aqueous zinc-ion battery, *Energy Storage Mater.*, 2020, **24**, 394–401.

113 L. Ren, G. Yu, H. Xu, W. Wang, Y. Jiang, M. Ji and S. Li, Doping-Induced Static Activation of MnO_2 Cathodes for Aqueous Zn-Ion Batteries, *ACS Sustain. Chem. Eng.*, 2021, **9**, 12223–12232.

114 F. Kataoka, T. Ishida, K. Nagita, V. Kumbhar, K. Yamabuki and M. Nakayama, Cobalt-Doped Layered MnO_2 Thin Film Electrochemically Grown on Nitrogen-Doped Carbon Cloth for Aqueous Zinc-Ion Batteries, *ACS Appl. Energy Mater.*, 2020, **3**, 4720–4726.

115 Y.-Y. Liu, G.-Q. Yuan, X.-Y. Wang, J.-P. Liu, Q.-Y. Zeng, X.-T. Guo, H. Wang, C.-S. Liu and H. Pang, Tuning electronic structure of ultrathin V_6O_{13} nanobelts via nickel doping for aqueous zinc-ion battery cathodes, *Chem. Eng. J.*, 2022, **428**, 132538.

116 S. Deng, H. Li, B. Chen, Z. Xu, Y. Jiang, C. Li, W. Xiao and X. Yan, High performance of Mn-doped VO_2 cathode for aqueous zinc-ion batteries: an insight into Zn^{2+} storage mechanism, *Chem. Eng. J.*, 2023, **452**, 139115.

117 V. T. Nguyen, F. N. I. Sari, B. W. Saputro and J.-M. Ting, Structural and defect modulations of co-precipitation synthesized high-entropy Prussian blue analogue nanocubes via Cu/Zn co-doping for enhanced electrochemical performance, *J. Mater. Chem. A*, 2023, **11**, 19483–19495.

118 D. Zhang, J. Cao, X. Zhang, N. Insin, S. Wang, J. Han, Y. Zhao, J. Qin and Y. Huang, Inhibition of Manganese Dissolution in Mn_2O_3 Cathode with Controllable Ni^{2+} Incorporation for High-Performance Zinc Ion Battery, *Adv. Funct. Mater.*, 2021, **31**, 2009412.

119 F. Gao, W. Shi, B. Jiang, Z. Xia, L. Zhang and Q. An, Ni/Fe Bimetallic Ions Co-Doped Manganese Dioxide Cathode Materials for Aqueous Zinc-Ion Batteries, *Batteries*, 2023, **9**, 50.

120 Z. Wu, F. Ye, Q. Liu, R. Pang, Y. Liu, L. Jiang, Z. Tang and L. Hu, Simultaneous Incorporation of V and Mn Element into Polyanionic NASICON for High Energy-Density and Long-Lifespan Zn-Ion Storage, *Adv. Energy Mater.*, 2022, **12**, 2200654.

121 Y. Zhang, Y. Liu, Z. Liu, X. Wu, Y. Wen, H. Chen, X. Ni, G. Liu, J. Huang and S. Peng, MnO_2 cathode materials with the improved stability via nitrogen doping for aqueous zinc-ion batteries, *J. Energy Chem.*, 2022, **64**, 23–32.

122 Y. Zhao, P. Zhang, J. Liang, X. Xia, L. Ren, L. Song, W. Liu and X. Sun, Uncovering sulfur doping effect in MnO_2 nanosheets as an efficient cathode for aqueous zinc ion battery, *Energy Storage Mater.*, 2022, **47**, 424–433.

123 Y. Zhao, R. Zhou, Z. Song, X. Zhang, T. Zhang, A. Zhou, F. Wu, R. Chen and L. Li, Interfacial Designing of MnO_2 Half-Wrapped by Aromatic Polymers for High-Performance Aqueous Zinc-Ion Batteries, *Angew. Chem., Int. Ed.*, 2022, **61**, e202212231.

124 H. Liu, L. Jiang, B. Cao, H. Du, H. Lu, Y. Ma, H. Wang, H. Guo, Q. Huang, B. Xu and S. Guo, Van der Waals Interaction-Driven Self-Assembly of V_2O_5 Nanoplates and MXene for High-Performing Zinc-Ion Batteries by Suppressing Vanadium Dissolution, *ACS Nano*, 2022, **16**, 14539–14548.

125 Y. Dai, C. Zhang, J. Li, X. Gao, P. Hu, C. Ye, H. He, J. Zhu, W. Zhang, R. Chen, W. Zong, F. Guo, I. P. Parkin, D. J. L. Brett, P. R. Shearing, L. Mai and G. He, Inhibition of Vanadium Cathodes Dissolution in Aqueous Zn-Ion Batteries, *Adv. Mater.*, 2024, **36**, 2310645.

126 Y. Geng, L. Pan, Z. Peng, Z. Sun, H. Lin, C. Mao, L. Wang, L. Dai, H. Liu, K. Pan, X. Wu, Q. Zhang and Z. He, Electrolyte additive engineering for aqueous Zn ion batteries, *Energy Storage Mater.*, 2022, **51**, 733–755.

127 C. Qiu, X. Zhu, L. Xue, M. Ni, Y. Zhao, B. Liu and H. Xia, The function of Mn^{2+} additive in aqueous electrolyte for Zn/δ-MnO_2 battery, *Electrochim. Acta*, 2020, **351**, 136445.

128 V. Soundharrajan, B. Sambandam, S. Kim, S. Islam, J. Jo, S. Kim, V. Mathew, Y.-k. Sun and J. Kim, The dominant role of Mn^{2+} additive on the electrochemical reaction in $ZnMn_2O_4$ cathode for aqueous zinc-ion batteries, *Energy Storage Mater.*, 2020, **28**, 407–417.

129 Y. Zhang, H. Li, S. Huang, S. Fan, L. Sun, B. Tian, F. Chen, Y. Wang, Y. Shi and H. Y. Yang, Rechargeable Aqueous Zinc-Ion Batteries in $MgSO_4/ZnSO_4$ Hybrid Electrolytes, *Nano-Micro Lett.*, 2020, **12**, 60.

130 L. Wang, S. Yan, C. D. Quilty, J. Kuang, M. R. Dunkin, S. N. Ehrlich, L. Ma, K. J. Takeuchi, E. S. Takeuchi and A. C. Marschilok, Achieving Stable Molybdenum Oxide Cathodes for Aqueous Zinc-Ion Batteries in Water-in-Salt Electrolyte, *Adv. Mater. Interfaces*, 2021, **8**, 2002080.

131 L. Zhang, I. A. Rodríguez-Pérez, H. Jiang, C. Zhang, D. P. Leonard, Q. Guo, W. Wang, S. Han, L. Wang and X. Ji, $ZnCl_2$ "Water-in-Salt" Electrolyte Transforms the Performance of Vanadium Oxide as a Zn Battery Cathode, *Adv. Funct. Mater.*, 2019, **29**, 1902653.

132 S. Chen, Y. Ying, L. Ma, D. Zhu, H. Huang, L. Song and C. Zhi, An asymmetric electrolyte to simultaneously meet contradictory requirements of anode and cathode, *Nat. Commun.*, 2023, **14**, 2925.

133 Q. Pang, H. Zhao, R. Lian, Q. Fu, Y. Wei, A. Sarapulova, J. Sun, C. Wang, G. Chen and H. Ehrenberg, Understanding the mechanism of byproduct formation

with in operando synchrotron techniques and its effects on the electrochemical performance of VO_2(B) nanoflakes in aqueous rechargeable zinc batteries, *J. Mater. Chem. A*, 2020, **8**, 9567–9578.

134 J. S. Ko, P. P. Paul, G. Wan, N. Seitzman, R. H. DeBlock, B. S. Dunn, M. F. Toney and J. Nelson Weker, NASICON $Na_3V_2(PO_4)_3$ Enables Quasi-Two-Stage Na^+ and Zn^{2+} Intercalation for Multivalent Zinc Batteries, *Chem. Mater.*, 2020, **32**, 3028–3035.

135 X. Wang, S. Tan, X.-Q. Yang and E. Hu, Pair distribution function analysis: fundamentals and application to battery materials, *Chin. Phys. B*, 2020, **29**, 028802.

136 X. Shan, S. Kim, A. M. M. Abeykoon, G. Kwon, D. Olds and X. Teng, Potentiodynamics of the Zinc and Proton Storage in Disordered Sodium Vanadate for Aqueous Zn-Ion Batteries, *ACS Appl. Mater. Interfaces*, 2020, **12**, 54627–54636.

137 K. Zhu, S. Wei, H. Shou, F. Shen, S. Chen, P. Zhang, C. Wang, Y. Cao, X. Guo, M. Luo, H. Zhang, B. Ye, X. Wu, L. He and L. Song, Defect engineering on V_2O_3 cathode for long-cycling aqueous zinc metal batteries, *Nat. Commun.*, 2021, **12**, 6878.

138 C. S. Schnohr and M. C. Ridgway, in *X-Ray Absorption Spectroscopy of Semiconductors*, ed. C. S. Schnohr and M. C. Ridgway, Springer Berlin Heidelberg, Berlin, Heidelberg, 2015, pp. 1–26, DOI: 10.1007/978-3-662-44362-0_1.

139 D. Liu, Z. Shadike, R. Lin, K. Qian, H. Li, K. Li, S. Wang, Q. Yu, M. Liu, S. Ganapathy, X. Qin, Q.-H. Yang, M. Wagemaker, F. Kang, X.-Q. Yang and B. Li, Review of Recent Development of In Situ/Operando Characterization Techniques for Lithium Battery Research, *Adv. Mater.*, 2019, **31**, 1806620.

140 N. Zhang, F. Cheng, Y. Liu, Q. Zhao, K. Lei, C. Chen, X. Liu and J. Chen, Cation-Deficient Spinel $ZnMn_2O_4$ Cathode in $Zn(CF_3SO_3)_2$ Electrolyte for Rechargeable Aqueous Zn-Ion Battery, *J. Am. Chem. Soc.*, 2016, **138**, 12894–12901.

141 Y. Wang, S. Wei, Z.-H. Qi, S. Chen, K. Zhu, H. Ding, Y. Cao, Q. Zhou, C. Wang, P. Zhang, X. Guo, X. Yang, X. Wu and L. Song, Intercalant-induced V t_{2g} orbital occupation in vanadium oxide cathode toward fast-charging aqueous zinc-ion batteries, *Proc. Natl. Acad. Sci. U.S.A.*, 2023, **120**, e2217208120.

142 F. Wan, Y. Zhang, L. Zhang, D. Liu, C. Wang, L. Song, Z. Niu and J. Chen, Reversible Oxygen Redox Chemistry in Aqueous Zinc-Ion Batteries, *Angew. Chem., Int. Ed.*, 2019, **58**, 7062–7067.

143 X. Wang, Z. Wang, C. Zhu, L. Zheng, Z. Wu, Y. Song, F. Wan and X. Guo, Unlocking Anionic Redox by Breaking Metal–Oxygen Bonds in Aqueous Zinc Batteries, *ACS Energy Lett.*, 2023, **8**, 4547–4554.

144 G. Fang, S. Liang, Z. Chen, P. Cui, X. Zheng, A. Pan, B. Lu, X. Lu and J. Zhou, Simultaneous Cationic and Anionic Redox Reactions Mechanism Enabling High-Rate Long-Life Aqueous Zinc-Ion Battery, *Adv. Funct. Mater.*, 2019, **29**, 1905267.

145 F. Zhao, J. Li, A. Chutia, L. Liu, L. Kang, F. Lai, H. Dong, X. Gao, Y. Tan, T. Liu, I. P. Parkin and G. He, Highly stable manganese oxide cathode material enabled by Grotthuss topochemistry for aqueous zinc ion batteries, *Energy Environ. Sci.*, 2024, **17**, 1497–1508.

146 J. Cao, D. Zhang, Y. Yue, X. Yang, C. Yang, J. Niu, Z. Zeng, P. Kidkhunthod, S. Wannapaiboon, X. Zhang, J. Qin and J. Lu, Unveiling the X-Ray Absorption Chemistry of $H_{3.78}V_6O_{13}$ Cathode for Aqueous Zinc-Ion Batteries, *Adv. Funct. Mater.*, 2023, **33**, 2307270.

147 S. Zhao, X. Wu, J. Zhang, C. Li, Z. Cui, W. Hu, R. Ma and C. Li, Biomass-derived porous carbon-supported single-atomic cobalt toward high-performance aqueous zinc-sulfur batteries at room temperature, *J. Energy Chem.*, 2024, **95**, 325–335.

148 L. Ma, G. Zhu, Z. Wang, A. Zhu, K. Wu, B. Peng, J. Xu, D. Wang and Z. Jin, Long-Lasting Zinc–Iodine Batteries with Ultrahigh Areal Capacity and Boosted Rate Capability Enabled by Nickel Single-Atom Electrocatalysts, *Nano Lett.*, 2023, **23**, 5272–5280.

149 B. Deng and X. Ju, in *Advanced X-ray Imaging of Electrochemical Energy Materials and Devices*, ed. J. Wang, Springer Singapore, Singapore, 2021, pp. 115–140, DOI: 10.1007/978-981-16-5328-5_6.

150 D. Wu, L. M. Housel, S. J. Kim, N. Sadique, C. D. Quilty, L. Wu, R. Tappero, S. L. Nicholas, S. Ehrlich, Y. Zhu, A. C. Marschilok, E. S. Takeuchi, D. C. Bock and K. J. Takeuchi, Quantitative temporally and spatially resolved X-ray fluorescence microprobe characterization of the manganese dissolution-deposition mechanism in aqueous Zn/α-MnO_2 batteries, *Energy Environ. Sci.*, 2020, **13**, 4322–4333.

151 M. Ebner, F. Marone, M. Stampanoni and V. Wood, Visualization and Quantification of Electrochemical and Mechanical Degradation in Li Ion Batteries, *Science*, 2013, **342**, 716–720.

152 S. Kumar, V. Verma, R. Chua, H. Ren, P. Kidkhunthod, C. Rojviriya, S. Sattayaporn, F. M. F. de Groot, W. Manalastas and M. Srinivasan, Multiscalar Investigation of $FeVO_4$ Conversion Cathode for a Low Concentration $Zn(CF_3SO_3)_2$ Rechargeable Zn-Ion Aqueous Battery, *Batteries Supercaps*, 2020, **3**, 619–630.

153 J. Fujii, in *Compendium of Surface and Interface Analysis*, ed. The Surface Science Society, Springer Singapore, Singapore, 2018, pp. 707–712, DOI: 10.1007/978-981-10-6156-1_114.

154 S. Wei, C. Wang, S. Chen, P. Zhang, K. Zhu, C. Wu, P. Song, W. Wen and L. Song, Dial the Mechanism Switch of VN from Conversion to Intercalation toward Long Cycling Sodium-Ion Battery, *Adv. Energy Mater.*, 2020, **10**, 1903712.

155 S. Wei, S. Chen, X. Su, Z. Qi, C. Wang, B. Ganguli, P. Zhang, K. Zhu, Y. Cao, Q. He, D. Cao, X. Guo, W. Wen, X. Wu, P. M. Ajayan and L. Song, Manganese buffer induced high-performance disordered MnVO cathodes in zinc batteries, *Energy Environ. Sci.*, 2021, **14**, 3954–3964.

156 M. Görlin, D. O. Ojwang, M.-T. Lee, V. Renman, C.-W. Tai and M. Valvo, Aging and Charge Compensation Effects of the Rechargeable Aqueous Zinc/Copper Hexacyanoferrate

Battery Elucidated Using In Situ X-ray Techniques, *ACS Appl. Mater. Interfaces*, 2021, **13**, 59962–59974.

157 Y. Sun, Z. Lian, Z. Ren, Z. Yao, Y. Yin, P. Huai, F. Zhu, Y. Huang, W. Wen, X. Li, R. Tai and D. Zhu, Proton-Dominated Reversible Aqueous Zinc Batteries with an Ultraflat Long Discharge Plateau, *ACS Nano*, 2021, **15**, 14766–14775.

158 D. Wu, S. T. King, N. Sadique, L. Ma, S. N. Ehrlich, S. Ghose, J. Bai, H. Zhong, S. Yan, D. C. Bock, E. S. Takeuchi, A. C. Marschilok, L. M. Housel, L. Wang and K. J. Takeuchi, Operando investigation of aqueous zinc manganese oxide batteries: multi-stage reaction mechanism revealed, *J. Mater. Chem. A*, 2023, **11**, 16279–16292.

159 D. Wu, L. M. Housel, S. T. King, Z. R. Mansley, N. Sadique, Y. Zhu, L. Ma, S. N. Ehrlich, H. Zhong, E. S. Takeuchi, A. C. Marschilok, D. C. Bock, L. Wang and K. J. Takeuchi, Simultaneous Elucidation of Solid and Solution Manganese Environments via Multiphase Operando Extended X-ray Absorption Fine Structure Spectroscopy in Aqueous Zn/MnO_2 Batteries, *J. Am. Chem. Soc.*, 2022, **144**, 23405–23420.

160 V. R. Kankanallu, X. Zheng, D. Leschev, N. Zmich, C. Clark, C.-H. Lin, H. Zhong, S. Ghose, A. M. Kiss, D. Nykypanchuk, E. Stavitski, E. S. Takeuchi, A. C. Marschilok, K. J. Takeuchi, J. Bai, M. Ge and Y.-c. K. Chen-Wiegart, Elucidating a dissolution–deposition reaction mechanism by multimodal synchrotron X-ray characterization in aqueous Zn/MnO_2 batteries, *Energy Environ. Sci.*, 2023, **16**, 2464–2482.

161 Y. Dai, X. Liao, R. Yu, J. Li, J. Li, S. Tan, P. He, Q. An, Q. Wei, L. Chen, X. Hong, K. Zhao, Y. Ren, J. Wu, Y. Zhao and L. Mai, Quicker and More Zn2+ Storage Predominantly from the Interface, *Adv. Mater.*, 2021, **33**, 2100359.

162 L. Wang, J. Yan, Y. Hong, Z. Yu, J. Chen and J. Zheng, Ultrahigh-rate and ultralong-life aqueous batteries enabled by special pair-dancing proton transfer, *Sci. Adv.*, 2023, **9**, eadf4589.